A mechanistic ecohydrological model to investigate complex interactions in cold and warm water-controlled environments: 1. Theoretical framework and plot-scale analysis

S. Fatichi,[1,2,3] V. Y. Ivanov,[2] and E. Caporali[1]

[1]   Numerous studies have explored the role of vegetation in controlling and mediating hydrological states and fluxes at the level of individual processes, which has led to improvements in our understanding of plot-scale dynamics. Relatively less effort has been directed toward spatially-explicit studies of vegetation-hydrology interactions at larger scales of a landscape. Only few continuous, process-oriented ecohydrological models had been proposed with structures of varying complexity. This study contributes to their further evolution and presents a novel ecohydrological model, *Tethys-Chloris*. The model synthesizes the state-of-the-art knowledge on individual processes and coupling mechanisms drawn from the disciplines of hydrology, plant physiology, and ecology. Specifically, the model reproduces all essential components of the hydrological cycle: it resolves the mass and energy budgets in the atmospheric surface layer at the hourly scale, while representing up to two layers of vegetation; it includes a module of snowpack evolution; it describes the saturated and unsaturated soil water dynamics, processes of runoff generation and flow routing. The component of vegetation dynamics parameterizes life cycle processes of different plant functional types, including photosynthesis, phenology, carbon allocation, and tissue turnover. This study presents a confirmation of the long-term, plot-scale model performance by simulating two types of ecosystems corresponding to different climate conditions. A consistent and highly satisfactory model skill in reproducing the energy and water budgets as well as physiological cycles of plants with minimum calibration overhead is demonstrated. Furthermore, these applications demonstrate that the model permits the identification of data types and observation frequencies crucial for appropriate evaluation of modeled dynamics. More importantly, through a synthesis of a wide array of process representations, the model ensures that climate, soil, vegetation, and topography collectively identify essential modes controlling ecohydrological systems, i.e., that satisfactory performance is a result of appropriate mimicking of internal processes.

1. Introduction

[2]   Watershed-scale hydrological modeling has a long history and dates back almost half a century, when arguably the first model, the "*Stanford Watershed Model*" [*Crawford and Linsley*, 1966] was implemented. Over the years, many other conceptual and physically based distributed models have been developed both at the hillslope and watershed-level scales [e.g., *Freeze*, 1971, 1972; *Beven and Kirkby*, 1979; *Abbott et al.*, 1986a, 1986b]. Major recent advances have included the explicit representation of topography and feedbacks from the atmospheric boundary layer and vegetation dynamics [*Tague and Band*, 2004; *Rigon et al.*, 2006; *Maxwell et al.*, 2007; *Ivanov et al.*, 2008].

[3]   Emphasis on vegetation as a dynamic component of the Earth system has been of particular interest for several reasons. By modifying boundary conditions at the land surface, vegetation exerts seasonal and long-term

[1]Department of Civil and Environmental Engineering, University of Florence, Florence, Italy.
[2]Department of Civil and Environmental Engineering, University of Michigan, Ann Arbor, Michigan, USA.
[3]Institute of Environmental Engineering, ETH Zürich, Zurich, Switzerland.

controls on the hydrological response through its effect on the water, momentum, and energy exchanges; in turn, water availability influences vegetation growth and plant performance [*Rodriquez-Iturbe et al.*, 1999; *Rodriguez-Iturbe*, 2000; *Rodriguez-Iturbe et al.*, 2001; *Eagleson*, 2002; *Bonan*, 2002; *Arora*, 2002; *Bond*, 2003; *Rodriguez-Iturbe and Porporato*, 2004; *Daly and Porporato*, 2005; *Chapin et al.*, 2008; *Bonan*, 2008; *Tague*, 2009]. Although many studies have led to the contributions in understanding of specific mechanisms, patterns, and behaviors controlling ecohydrological systems [e.g., *Guswa et al.*, 2002; *Daly et al.*, 2004; *Caylor et al.*, 2005; *Montaldo et al.*, 2008; *Botter et al.*, 2008], relatively less effort has been devoted to the development of comprehensive, mechanistic ecohydrological models capable of simulating long-term dynamics in a spatially explicit manner [*Tague and Band*, 2004; *Ivanov et al.*, 2008]. This work contributes to this type of developments by integrating state-of-the-art descriptions of hydrological and plant biochemical processes in a novel ecohydrological model, "Tethys-Chloris" (T&C).

[4] In presenting a new model, two questions naturally arises: *why is there a need to develop a new numerical tool?*, and *what is new in such a tool?* These questions require a prompt answer.

[5] Despite a large number of existing watershed models (e.g., reviews by *Singh and Woolhiser* [2002], *Reed et al.* [2004], and *Kampf and Burges* [2007]), only a small fraction can be regarded as those based on physical principles of water flow in the surface and subsurface environments, allowing transient solutions (see discussions in *Paniconi and Wood* [1993], *Ivanov et al.* [2004b], *Loague and VanderKwaak* [2004], *Maxwell and Miller* [2005], *Kollet and Maxwell* [2006], *Loague et al.* [2006], *Qu and Duffy* [2007], *Ebel et al.* [2008], *Kumar et al.* [2010], *Camporese et al.* [2010], and *Mirus et al.* [2011]). Furthermore, few models were designed to cross the boundary of the hydrological discipline to include the processes of vegetation dynamics, atmospheric boundary layer, and/or biogeochemistry. A limited understanding of a number of hydrological and ecological processes, their interdependencies, heterogeneities in space, required fine scales of representation, the lack of appropriate methods for specifying initial and boundary conditions, and required computational resources [*Kollet et al.*, 2010; *Wood et al.*, 2011] have in particular hampered the development of complex models. Yet, there are both practical and theoretical reasons for stimulating further evolution of these numerical tools.

[6] From a theoretical stand point, a mechanistic model should represent a rigorous mathematical formulation reflecting the state-of-the-art understanding of system processes. This representation of governing laws and linkages among system elements is fundamental for establishing the basis for subsequent model developments and improvements as well as for guiding observational practices. Practically, a mechanistic ecohydrological model offers the opportunity of investigating principal controls on an ecosystem and hydrological response, avoiding gross, over-lumped representations typical of simplified approaches. Such a model can elucidate feedback mechanisms and permit a quantitative analysis that would be difficult to capture with idealized cases of analytical solutions or plot-scale analyses.

[7] Predominantly physically-based formulations with measurable states and fluxes are used in the framework of Tethys-Chloris. Model components simulating processes where our understanding is still limited, such as plant carbon relations and phenology, are described with semi-empirical equations. By integrating a wide spectrum of dynamics within a mechanistic, process-oriented formulation, Tethys-Chloris represents a novel development. Specifically, while many components are descriptions of "classical" hydrological processes (e.g., infiltration, interception, runoff generation, surface flow, etc.), their coupling methodology, a range of new process representations, and their integration within the same computational structure are unusual for a hydrological model. The most significant novelty is the capability to combine an explicit treatment of vegetation dynamics with the spatial and temporal variability of hydrological states and fluxes in a variety of landscapes and climates. By resolving both fine and coarse spatio-temporal scales, Tethys-Chloris permits coupled modeling of dynamic vegetation-hydrology feedbacks. Thus the model is a substantial, innovative evolution of existing alternatives, such as conceptual and data-driven approaches [e.g, *Emanuel et al.*, 2010; *Abdelnour et al.*, 2011; *Istanbulluoglu et al.*, 2011; *Thompson et al.*, 2011b] and complements the few existing mechanistic watershed scale ecohydrological models, *tRIBS+VEGGIE* [*Ivanov et al.*, 2004a, 2004b; *Ivanov*, 2006; *Ivanov et al.*, 2008] and *RHESSys* [*Band et al.*, 1993; *Mackay and Band*, 1997; *Tague and Band*, 2004].

[8] The framework of coupled interactions has been truly fundamental for Tethys-Chloris implementation: not only hydrological fluxes are mediated by vegetation dynamics but the latter, in turn, exert controls on hydrological processes. Different temporal scales are represented, ranging from the sub-daily plant control of leaf stomatal aperture, to the seasonal control of vegetation phenological transitions on soil moisture and its redistribution [*Ivanov et al.*, 2010], and up to the annual or multi-year adaptation of vegetation cover to environmental conditions imposed by climate, soil, and topography. Tethys-Chloris resolves multi-scale vegetation dynamics based on modeling plant carbon balance at fine (sub-daily, hourly) time and space scales. Only empirical understanding of plant function is currently available and the model presents a number of novel developments and simulation solutions extending beyond conventional approaches. For instance, these include an explicit simulation of carbon allocation to reserves with a consequent mobilization of carbohydrates at the onset of growing season and a parameterization of green aboveground tissue aging. Furthermore, the representation of plant carbon balance, tissue turnover, and phenology are the subject of ongoing research in plant ecology and demand for new insights in modeling solutions. Most recent findings in plant

physiology research have been accounted for in Tethys-Chloris.

[9] The model has been explicitly designed to simulate the ecohydrological dynamics of both warm and cold water-controlled environments. The difference in major hydrological drivers and vegetation types that occur across temperature and precipitation gradients is a great challenge for any model. They demand the simulation of a large variety of ecological and hydrological components, as detailed in this paper and the auxiliary material.[1] To author's knowledge, Tethys-Chloris is the first comprehensive ecohydrological model that explicitly includes the effects of snow dynamics.

[10] Finally, the envisioned scope of applications targeted by Tethys-Chloris is ultimately shaped by ecohydrological dynamics occurring in complex terrain. When resolved at appropriate spatial and temporal scales, the model is capable of mimicking complex patterns imposed by the watershed morphology. For example, through lateral transfer of water and local and remote topographic effects on incident radiation, the differences in ecohydrological behavior of upslope/downslope, north/south exposed areas (such as vegetation productivity, aquifer recharge, evapotranspiration, etc.) can be explicitly resolved. While at its foundation the model operates at the local-scale and with hourly representation of processes, the integration of computational elements into a scaleable structure leads to the emergence of meaningful ecohydrological dynamics over a variety of temporal and spatial scales extending to the entire watershed domain.

[11] In this paper, the theoretical background, the design considerations, and the overall structure of "Tethys-Chloris" are presented. The capabilities of the model in reproducing long-term, plot-scale ecohydrological dynamics for two types of ecosystems corresponding to different climate conditions are also demonstrated. In a companion paper [*Fatichi et al.*, 2012], a detailed confirmation of the model performance is discussed, illustrating the model potential for simulating distributed dynamics at larger watershed scales and presenting a number of opportunities for future ecohydrological studies.

2. Model Overview

[12] The model simulates the energy and water budgets and the physiological cycle of plants, representing different carbon compartments. Vegetated and non-vegetated surfaces can be simultaneously present in a given element; these surfaces can be snow-covered or snow-free.

[13] Multiple processes are represented in the model that interact with each other in a dynamic fashion, mimicking a two-way coupled vegetation-hydrology system. An outline of the simulated hydrological processes is sketched in Figure 1. The coupling among various plant life regulatory mechanisms is illustrated in Figure 2. The simulated components are also listed in

the following. Their detailed description is provided in the auxiliary material.

[14] *Hydrological components*: (1) absorption, reflection, and transmittance of solar shortwave radiation and atmospheric longwave radiation; (2) sensible and latent heat fluxes, ground heat flux, and heat sink/source associated with precipitation, partition of latent heat into evaporation and transpiration; (3) resistance schemes for water and energy fluxes, including aerodynamic, leaf boundary layer, soil, and stomatal resistances; (4) snow hydrology component, including snowpack energy balance, snowmelt, and snow interception by canopy; (5) interception, throughfall, and stem flow; (6) infiltration and water movement in a multi-layer soil, including unsaturated and saturated zone dynamics, and runoff formation; (7) surface flow routing.

[15] *Vegetation dynamics components*: (1) photosynthesis and plant respiration; (2) carbon allocation and translocation; (3) tissue turnover and stress-induced foliage loss; (4) vegetation phenology.

[16] The hydrological budget is formulated at an *hourly* time scale to preserve sub-daily meteorological dynamics. Most vegetation dynamics are simulated at the daily time scale, however biochemical processes of photosynthesis and stomatal physiology are computed at the hourly time scale, as a necessary component affecting the hydrological budget. Other modules may operate at the sub-hourly resolution, e.g., the subsurface water dynamics are formulated to have an adaptive time stepping (minutes). The surface flow routing uses a 2 [*s*] internal time step. Mass and energy budgets are conserved at their respective computational steps.

[17] A complete list of meteorological inputs, simulated fluxes, and states as well as model parameters is presented in Tables 1–3. For a detailed description of these variables and parameters, the reader is referred to the auxiliary material. Table 3 includes expected realistic ranges for all of the parameters used in the model.

3. Basic Computational Element Geometry and Surface Composition

[18] The dynamics of each computational element are resolved using locally simulated conditions. Spatial interactions are introduced by considering the surface and subsurface water transfers among elements (Figure 3a) that affect the soil moisture states and, in turn, impact local dynamics via the coupled energy-water interactions. Shading cast by remote terrain is also considered since it can influence the incoming energy. A quasi-three-dimensional representation of dynamics in a given domain is thus achieved.

[19] In a distributed watershed model, the basin domain is typically represented using a number of elementary computational structures [*Kampf and Burges*, 2007]. These are referred to here as *basic computational elements*, implying smallest elements for which the model computes energy and water fluxes.

[20] Basic computational elements can be represented in different ways, such as sub-watersheds, contour-based

---

[1]Auxiliary materials are available in the HTML. doi:10.1029/2011MS000086
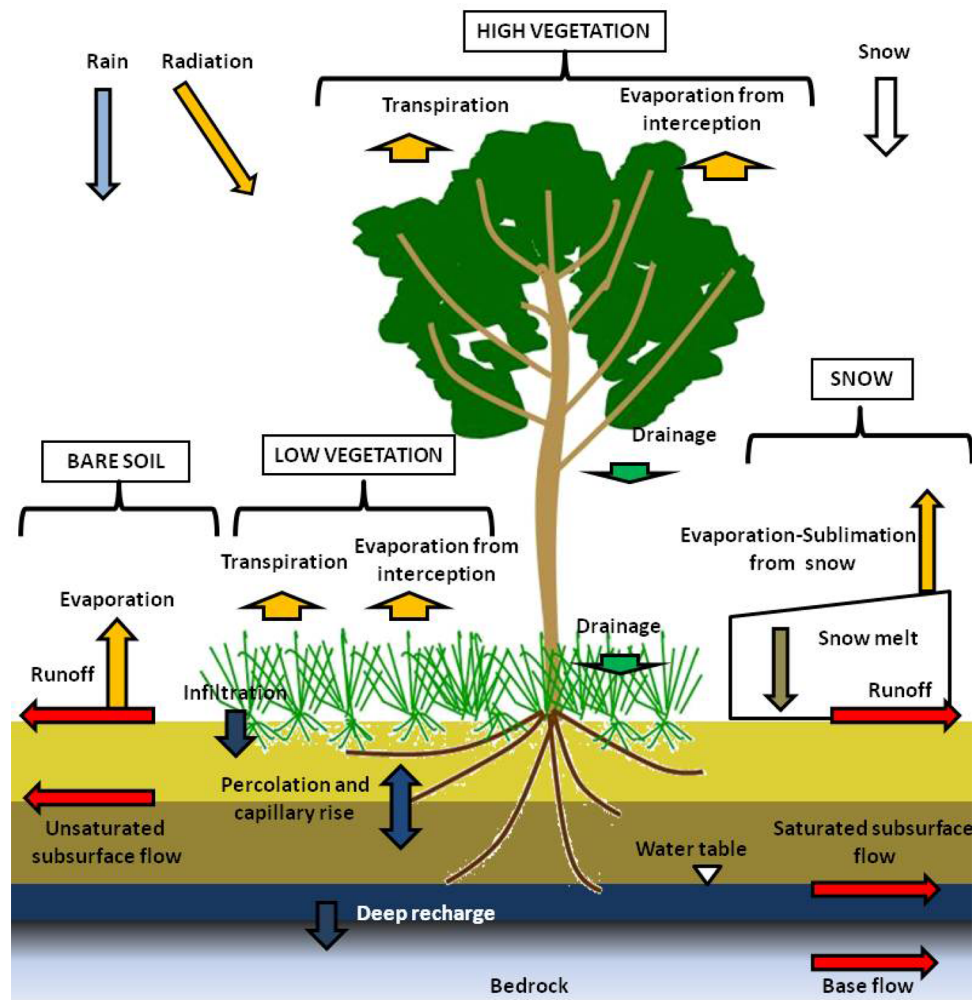
Figure 1.   A diagram of components included in the hydrological and energy balance models.

streamtubes, triangulated irregular networks (TIN), or grid domains [*Tucker et al.*, 2001; *Menduni et al.*, 2002; *Ivanov et al.*, 2004a; *Vivoni et al.*, 2005; *Kampf and Burges*, 2007; *Rulli*, 2010]. T&C uses a regular, square grid (Figure 3a). This type is known as Digital Elevation Model (DEM), or Digital Terrain Model (DTM) and has been widely used to describe watershed geometry [*O'Callaghan and Mark*, 1984; *Abbott et al.*, 1986b; *Wigmosta et al.*, 1994; *Bertoldi et al.*, 2006b]. While this is not a parsimonious computational choice, the pros and cons of the approach are well known and algorithms retrieving topographic and hydrologic features (e.g., slope, aspect, and curvature) from DEMs are advanced. The same holds true with regards to terrain parameters affecting incoming solar radiation [*Kumar et al.*, 1997; *Dubayah and Loechel*, 1997; *Rigon et al.*, 2006; *Ivanov et al.*, 2007; *Fatichi et al.*, 2011], or important hydrologic characteristics such as flow direction [*O'Callaghan and Mark*, 1984; *Tarboton*, 1997; *Orlandini et al.*, 2003; *Nardi et al.*, 2008].

[21]   Basic computational elements that compose a watershed domain can be characterized by topographic features. Each element is represented by a square with typical dimensions of 25–2500 m^2. The slope and aspect are calculated on the basis of a DEM along with the sky-view factor, the shadow effect (also time dependent), and the terrain configuration factor [*Bertoldi et al.*, 2006a; *Fatichi*, 2010; *Fatichi et al.*, 2011]. Energy fluxes are only computed vertically and no lateral energy advection is considered.

[22]   The vertical reference system of each element is represented by the normal to the surface, *n*, which is used to define surface and subsurface attributes of an element (e.g., soil layer mesh). The state variables and fluxes of the one-dimensional equations are also a function of the normal direction *n* (although for simplicity of presentation, the dependence on *n* is omitted later in the text).

[23]   Basic computational elements of T&C can account for up to three different land cover types: vegetated areas, bare soil areas, and water. The model also computes snow cover that can alter the representation of land cover. The assumptions are as follows: (i) when snow is present on the ground, it covers bare soil areas; (ii) water surfaces are not allowed to hold snow, although they are allowed to freeze; and (iii) intercepted
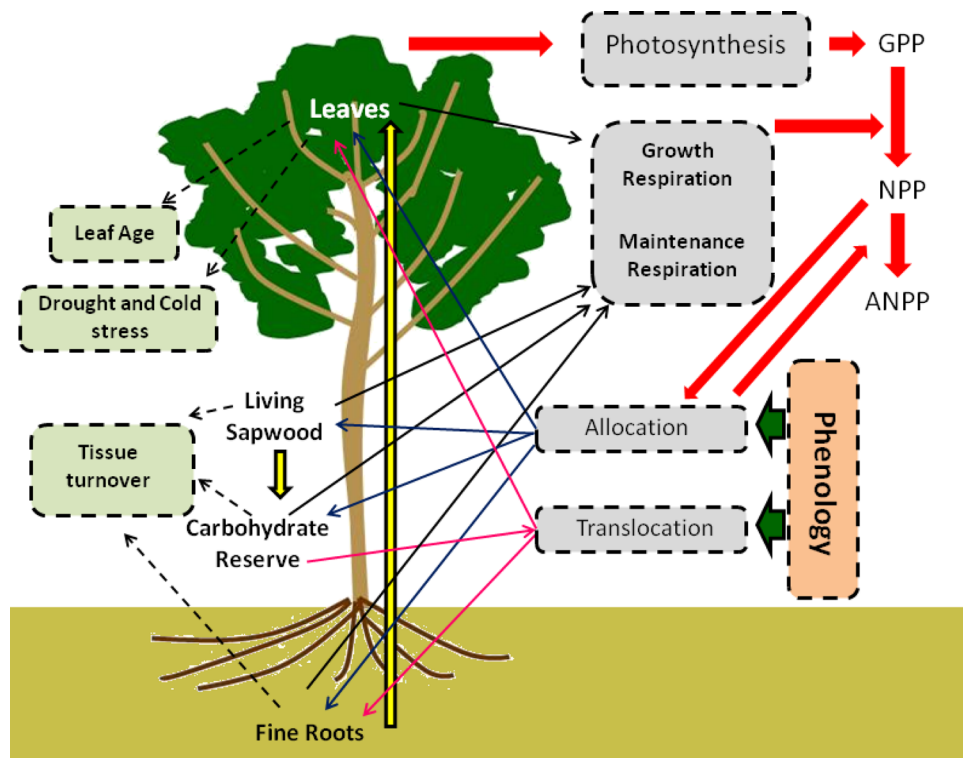
Figure 2. A conceptual diagram of carbon fluxes and the processes simulated by the model. The four carbon pools represent leaves, fine roots, living sapwood, and carbohydrate reserve. Boxes outlined with the dashed lines illustrate processes that affect carbon balance. The red arrows indicate general fluxes related to photosynthetic products. The blue solid-line arrows show allocation fluxes, while the magenta lines show translocation. The black dashed-line arrows indicate turnover from carbon pools. The yellow arrows indicate allometric constraint controls.

snow modifies radiative properties of vegetation and snow can eventually bury vegetation which is a function of relative heights of snow and vegetation. Further details are provided in the auxiliary material.

[24] Vegetated fraction of the basic computational element, C_{veg}, can include one or several vegetation types. Vegetation species that share the same life form, physiology, and structural attributes are described as Plant Functional Types (*PFT*) [*Bonan et al.*, 2002]. According to characteristics of vegetation species present in a given element, one or more PFTs can be

simulated. Furthermore, the model can consider both horizontal and vertical composition of vegetation patches.

[25] The vertical composition is realized using a concept of *Crown Area*. The latter represents an area occupied by one or two vertically "stacked" PFTs. It represents the surface projected area of tree crowns and is assumed to represent the area effectively occupied by grasses and shrubs. Up to two PFTs can be considered for a *Crown Area*: one representing overstory canopy, henceforth referred to as the *High-vegetation* (H_v) layer; and the other representing understory canopy, referred to as the *Low-vegetation* (L_v) layer. Each PFT is characterized by several structural vegetation attributes, such as leaf area index, *LAI* [m^2 *leaf area* m^{-2} PFT *area*], stem area index, *SAI* [m^2 *stem area* m^{-2} PFT *area*], canopy height, and root profile [*Bonan*, 1996; *Jackson et al.*, 1996; *White et al.*, 2000; *Feddes et al.*, 2001; *Schenk and Jackson*, 2002; *Collins and Bras*, 2007]. The "*PFT area*" corresponds to the *Crown Area*. LAI and SAI at the element scale are obtained by multiplying PFT-scale quantities by the relative *Crown Area* fractions, C_{crown}.

[26] The horizontal land cover composition of T&C accounts for different *Crown Areas* present in an element. In total, they occupy the entire vegetated fraction of a computational element. Patches of bare soil represent the remaining fraction, $1 - C_{veg}$. These fractions are used to weight the relative contributions of vegetation

Table 1. Meteorological Input Used for Forcing "Tethys-Chloris"

Variable	Description	Units
$R_{dir,\Lambda}$	Incoming direct beam shortwave radiation	[$W\,m^{-2}$]
$R_{dif,\Lambda}$	Incoming diffuse shortwave radiation	[$W\,m^{-2}$]
PAR_B	Incoming direct beam *Photosynthetically Active Radiation*	[$W\,m^{-2}$]
PAR_D	Incoming diffuse *Photosynthetically Active Radiation*	[$W\,m^{-2}$]
P_r	Precipitation	[$mm\,h^{-1}$]
T_a	Air temperature at a reference height	[$°C$]
e_a	Vapor pressure at a reference height	[Pa]
N	Cloud cover	[$-$]
P_{atm}	Atmospheric pressure	[Pa]
W_s	Wind speed at a reference height	[$m\,s^{-1}$]
c_a	Atmospheric CO_2 concentration	[Pa]

Table 2. A List of Principal Fluxes and States Simulated by "Tethys-Chloris"

Variable	Description	Units
	Energy and Mass Fluxes	
R_{abs}	Absorbed shortwave radiation	$[W\,m^{-2}]$
L_{abs}	Absorbed longwave radiation	$[W\,m^{-2}]$
PAR_{abs}	Absorbed *Photosynthetically Active Radiation*	$[W\,m^{-2}]$
R_n	Net radiation	$[W\,m^{-2}]$
H	Sensible heat	$[W\,m^{-2}]$
λE	Latent heat	$[W\,m^{-2}]$
G	Ground heat flux	$[W\,m^{-2}]$
Q_v	Incoming heat with precipitation	$[W\,m^{-2}]$
T_s	Prognostic surface temperature	$[°C]$
T_d	Ground temperature at damping depth	$[°C]$
$T_{H_v\,or\,L_v}$	Transpiration flux from vegetation	$[mm\,h^{-1}]$
E_g	Evaporation flux from ground under vegetation	$[mm\,h^{-1}]$
E_{bare}	Evaporation flux from bare soil	$[mm\,h^{-1}]$
E_{wat}	Evaporation flux from water surface	$[mm\,h^{-1}]$
$E_{sno,f\,or\,s}$	Evaporation/sublimation flux from snow in open surface and snow under vegetation	$[mm\,h^{-1}]$
$E_{In,H_v\,or\,L_v}$	Evaporation flux from intercepted water in canopy	$[mm\,h^{-1}]$
$\alpha_{soil,\Lambda}$	Albedo of ground	$[-]$
α_{sno}	Albedo of snow	$[-]$
$\alpha_{wat,\Lambda}$	Water albedo	$[-]$
ϵ_s	Emissivity of a generic surface	$[-]$
α_s	Absorptivity of a generic surface	$[-]$
$P_{r,liq}$	Liquid (rain) precipitation	$[mm\,h^{-1}]$
$P_{r,sno}$	Solid (snow) precipitation	$[mm\,h^{-1}]$
	Turbulent Regime/Resistances	
r_a	Aerodynamic resistance	$[s\,m^{-1}]$
r_a'	Undercanopy resistance	$[s\,m^{-1}]$
r_b	Leaf boundary layer resistance	$[s\,m^{-1}]$
r_{soil}	Soil resistance	$[s\,m^{-1}]$
r_s	Stomatal resistance	$[s\,m^{-1}]$
d	Zero-plane displacement height	$[m]$
z_{om}	Roughness length for momentum	$[m]$
z_{oh}	Roughness length for heat flux	$[m]$
z_{ow}	Roughness length for water vapor	$[m]$
α	Attenuation coefficient for undercanopy resistance	$[-]$
α'	Attenuation coefficient for leaf boundary layer conductance	$[-]$
$\hat{\alpha}$	Humidity equilibrium value for soil water content	$[-]$
	Biochemical Model of Photosynthesis	
A_{nC}	Net assimilation rate	$[\mu mol\,CO_2\,s^{-1}m^{-2}]$
R_{dC}	Dark respiration	$[\mu mol\,CO_2\,s^{-1}m^{-2}]$
A_C	Gross photosynthetic rate	$[\mu mol\,CO_2\,s^{-1}m^{-2}]$
V_{max}	Canopy maximum Rubisco capacity at 25°C	$[\mu mol\,CO_2\,s^{-1}m^{-2}]$
J_{max}	Canopy maximum electron transport capacity at 25°C	$[\mu mol\,Eq\,s^{-1}\,m^{-2}]$
V_m	Maximum Rubisco capacity at canopy scale after accounting for temperature dependence	$[\mu mol\,CO_2\,s^{-1}m^{-2}]$
J_m	Maximum electron transport capacity at canopy scale after accounting for temperature dependence	$[\mu mol\,Eq\,s^{-1}\,m^{-2}]$
J_{max}^L	Maximum electron transport capacity at 25°C at leaf scale	$[\mu mol\,Eq\,s^{-1}\,m^{-2}]$
θ_R	Soil water content available to roots	$[-]$
c_i	Partial pressure of intercellular CO_2	$[Pa]$
	Snow Hydrology	
C_{sno}	Boolean operator reflecting presence or absence of snow	$[0/1]$
S_{WE}	Snow water equivalent of ground snowpack	$[mm]$
$In_{S_{WE}}$	Snow water equivalent of intercepted snow in high-vegetation layer	$[W\,m^{-2}]$
dQ	Net energy flux input to snowpack	$[W\,m^{-2}]$
S_m	Snowmelt rate	$[mm]$
Q_{fm}	Heat release from melting (negative) or freezing (positive) of liquid water content held by snow	$[W\,m^{-2}]$
$U_{In_{S_{WE}}}$	Unloading of intercepted snow	$[mm]$
$In_{S_{WE}}^N$	Intercepted fresh snow	$[mm]$
$E_{In_{S_{WE}}}$	Sublimation/evaporation from intercepted snow	$[mm\,h^{-1}]$
$d_{w,sno}$	Fraction of canopy covered by snow	$[-]$
W_r	Water released from snowpack	$[mm]$
Sp_{wc}	Water content in snowpack	$[mm]$
S_{dep}	Snow depth	$[m]$
ρ_{sno}^{new}	Density of fresh snow	$[kg\,m^{-3}]$
ρ_{sno}	Snow density of ground snowpack	$[kg\,m^{-3}]$
Sp_{wc}^M	Maximum water holding capacity of snowpack	$[mm]$

Table 2. Continued

Variable	Description	Units
	Canopy Interception	
C_{fol}	Fraction of PFT area occupied by leaves and stems projected in vertical direction	[m^2 *vegetated area* m^{-2} *PFT area*]
In	Intercepted water stored in canopy	[mm]
$Dr_{H_v \, or \, L_v}$	Total drainage from a vegetation layer	[$mm \, h^{-1}$]
Dr_d	Rate of dripping from canopy	[$mm \, h^{-1}$]
Dr_s	Canopy drainage at saturation	[$mm \, h^{-1}$]
	Subsurface Water Dynamics	
q_{ins}	Total rate of influx of water to soil surface	[$mm \, h^{-1}$]
q_{runon}	Runon flux rate	[$mm \, h^{-1}$]
I_f^C	Infiltration capacity rate	[$mm \, h^{-1}$]
I_f	Actual infiltration rate	[$mm \, h^{-1}$]
R_H	Rate of infiltration excess runoff	[$mm \, h^{-1}$]
R_D	Rate of saturation excess runoff	[$mm \, h^{-1}$]
$Q_{l,in}$	Incoming subsurface lateral flux rate	[$mm \, h^{-1}$]
$Q_{l,out}$	Outgoing subsurface lateral flux rate	[$mm \, h^{-1}$]
L_{kb}	Leakage between vadose zone and bedrock, recharge to deep aquifers	[$mm \, h^{-1}$]
ρ_{cr}	Bulk density of seal	[$kg \, m^{-3}$]
E_K	Rainfall cumulative kinetic energy	[J mm^{-2}]
θ	Volumetric soil water content	[$-$]
$\Psi(\theta)$	Soil water potential	[mm] or [MPa]
$K_v(\theta)$	Unsaturated hydraulic conductivity	[$mm \, h^{-1}$]
Z_{wt}	Water table depth	[mm]
	Surface Water Dynamics	
R_{tot}	Overland runoff depth	[mm]
R_{ch}	Channel runoff depth	[mm]
y	Overland flow depth	[mm]
y_{ch}	Channel flow depth	[m]
U	Overland flow velocity	[$m \, s^{-1}$]
U_{ch}	Channel flow velocity	[$m \, s^{-1}$]
$\overrightarrow{R_{tot}}$	Routed fraction of R_{tot}	[mm]
$\overrightarrow{R_{ch}}$	Routed fraction of R_{ch}	[mm]
Q_{ov}	Overland discharge	[$mm \, h^{-1}$]
Q_{ch}	Channel discharge	[$mm \, h^{-1}$]
	Vegetation Productivity	
C_{leaf}	Green aboveground biomass (leaves or grass) carbon pool	[$gC \, m^{-2} \, PFT$]
C_{sapw}	Living sapwood carbon pool	[$gC \, m^{-2} \, PFT$]
C_{root}	Fine roots carbon pool	[$gC \, m^{-2} \, PFT$]
C_{hydr}	Carbohydrate reserve carbon pool	[$gC \, m^{-2} \, PFT$]
NPP	Net Primary Production	[$gC \, m^{-2} \, PFT \, day^{-1}$]
GPP	Gross Primary Production	[$gC \, m^{-2} \, PFT \, day^{-1}$]
$ANPP$	Above-ground Net Primary Production	[$gC \, m^{-2} \, PFT \, day^{-1}$]
R_A	Autotrophic respiration	[$gC \, m^{-2} \, PFT \, day^{-1}$]
R_g	Growth respiration	[$gC \, m^{-2} \, PFT \, day^{-1}$]
R_m	Maintenance respiration	[$gC \, m^{-2} \, PFT \, day^{-1}$]
R_{mS}	Living sapwood maintenance respiration	[$gC \, m^{-2} \, PFT \, day^{-1}$]
R_{mR}	Fine root maintenance respiration	[$gC \, m^{-2} \, PFT \, day^{-1}$]
R_{mH}	Carbohydrate reserve maintenance respiration	[$gC \, m^{-2} \, PFT \, day^{-1}$]
R_{mF}	Foliage maintenance respiration	[$gC \, m^{-2} \, PFT \, day^{-1}$]
N_s	Living sapwood carbon-nitrogen C:N mass ratio	[$gC \, gN^{-1}$]
N_r	Fine root carbon-nitrogen C:N mass ratio	[$gC \, gN^{-1}$]
	Carbon Allocation and Turnover	
f_l	Allocation fraction to green aboveground biomass	[$-$]
f_s	Allocation fraction to living sapwood	[$-$]
f_r	Allocation fraction to fine roots	[$-$]
f_h	Allocation fraction to carbohydrate reserves	[$-$]
f_f	Allocation fraction to fruit and flowers	[$-$]
T_{rC}	Carbohydrate translocation rate	[$gC \, m^{-2} \, PFT \, day^{-1}$]
S_{sapw}	Rate of turnover of sapwood to heartwood biomass	[$gC \, m^{-2} \, PFT \, day^{-1}$]
S_{root}	Tissue turnover of fine root biomass to litter	[$gC \, m^{-2} \, PFT \, day^{-1}$]
S_{leaf}	Tissue turnover of green aboveground biomass to litter	[$gC \, m^{-2} \, PFT \, day^{-1}$]
	Vegetation Phenology	
LAI	Leaf area index	[m^2 *leaf area* m^{-2} *ground area*]
A_{gL}	Leaf age	[day]
Φ	Phenology state	[1,…,4]
N_{LAI}	New leaf area onset over a time step dt	[m^2 *leaf area* m^{-2} *PFT area*]

Table 3. A List of Parameters Used in "Tethys-Chloris"

| Parameter	Description	Units	Typical Range
	Element Partition		
C_{veg}	Fraction of land cover occupied by vegetated areas	[−]	
C_{bare}	Fraction of land cover occupied by bare soil area	[−]	
C_{wat}	Fraction of land cover occupied by water	[−]	
n_c	Number of *Crown Areas*		
	Soil, Bedrock, Topography		
F_{san}	Fraction of sand	[−]	0–1
F_{cla}	Fraction of clay	[−]	0–1
P_{org}	Percentage of organic material	[%]	0–10
a_r	Soil anisotropy ratio	[−]	0–1000
K_{bot}	Conductivity of bedrock	[$mm\ h^{-1}$]	0–2
a_T	Area of basic element per unit contour length that drains through location	[mm]	
β_T	Element slope	[rad]	
w_{ch}	Channel width	[m]	
n_{hi}	Manning roughness coefficient for hillslopes	[$s\ m^{-1/3}$]	0.025–1.5
n_{ch}	Manning roughness coefficient for channels	[$s\ m^{-1/3}$]	0.01–0.05
	Soil Sealing		
$\Delta\rho*$	Maximum value of change in bulk density at soil surface reached after a long exposure to rainfall	[$kg\ m^{-3}$]	400
d_{cr}^*	Maximum value of seal thickness reached after a long exposure to rainfall	[mm]	10
C	Fitting parameter of soil seal effect	[$m^3\ kg^{-1}$]	$2.5\ 10^{-4}$
η_{cr}	Empirical parameter depending on soil-rainfall characteristics	[$mm^2\ J^{-1}$]	7000
ζ_{cr}	Empirical parameter depending on soil-rainfall characteristics	[$mm^2\ J^{-1}$]	3500
	Albedo and Roughness		
$\alpha_{sat\ \Lambda}$	Albedo of saturated soil	[−]	0.05–0.24
$\alpha_{dry\ \Lambda}$	Albedo of dry soil	[−]	0.10–0.48
α_{sno}^m	Minimum value of snow albedo	[−]	0.5
α_{sno}^M	Maximum value of snow albedo	[−]	0.85
z_{atm}	Reference height of meteorological observations	[m]	
	Snow Hydrology		
T_{min}	Threshold temperature below which all precipitation is considered to be snow	[$°C$]	(−1.5)–(0.0)
T_{max}	Threshold temperature above which all precipitation is considered to be rain	[$°C$]	(2.0)–(3.3)
$\bar{u}$	Unloading rate of intercepted snow	[h^{-1}]	$4.1\ 10^{-3}$
$\widehat{Sp}_{sno,In}$	Maximum snow load per unit of stem and leaf area	[$kg\ m^{-2}$]	5.9–6.6
ρ_{sno}^{M1}	Maximum density allowed for snow in melting conditions	[$kg\ m^{-3}$]	520
ρ_{sno}^{M2}	Maximum density allowed for snow in freezing conditions	[$kg\ m^{-3}$]	320
	Canopy Interception		
$S_{p,In}$	Specific water retained by vegetated area	[$mm\ m^2\ PFT\ area\ m^{-2}\ leaf\ area$]	0.1–0.4
K_c	Interception drainage rate coefficient	[$mm\ h^{-1}$]	0.06
g_c	Interception exponential decay parameter	[mm^{-1}]	3.7
	Vegetation Structural Characteristics		
H_c	Canopy height	[m]	0.1–100
SAI	Stem area index	[$m^2\ stem\ area\ m^{-2}\ ground\ area$]	0–0.5
d_{leaf}	Characteristic leaf dimension	[cm]	0.1–15
$Z_{root}(z)$	Root profile fractional density with depth z	[−]	
χ_L	Departure of leaf angles from a spherical angle distribution	[−]	(−0.30)–(0.25)
α_Λ	Leaf and stem reflectances	[−]	0.07–0.58
τ_Λ	Leaf and stem transmittances	[−]	0.001–0.38
Ξ	Broad vegetation category identifier	[−]	0–2
S_{LAI}	Specific leaf biomass area	[$m^2\ LAI\ gC^{-1}$]	0.005–0.05
	Photosynthesis		
Ψ_{ss}	Soil water potential at which stomatal closure begins	[MPa]	(−0.03)–(−1.0)
Ψ_{wp}	Soil water potential at full stomatal closure	[MPa]	(−1.0)–(−10.0)
K_N	Canopy nitrogen decay coefficient	[−]	0.15–0.5
φ_p	Photosynthesis pathway	C_3, C_4 or CAM	
V_{max}^L	Maximum Rubisco capacity at 25°C at leaf scale	[$\mu mol\ CO_2\ s^{-1}\ m^{-2}$]	10–150
O_i	Partial pressure of O_2	[Pa]	22290
H_a	Activation energy	[$kJ\ mol^{-1}$]	40–95
H_d	Deactivation energy	[$kJ\ mol^{-1}$]	200
ΔS	Entropy factor	[$kJ\ mol^{-1}\ K^{-1}$]	0.625–0.665

Table 3. Continued

Parameter	Description	Units	Typical Range
r_{jv}	Scaling factor between J_{max} and V_{max}	$[\mu mol\ Eq\ \mu mol\ CO_2^{-1}]$	1.5–2.5
ϵ	Intrinsic quantum efficiency	$[\mu mol\ CO_2\ \mu mol^{-1}\ photons]$	0.040–0.090
g_{0,CO_2}	Cuticular conductance	$[mol\ CO_2\ m^{-2}\ leaf\ s^{-1}]$	0.005–0.04
a	Empirical parameter linking A_{nC} to g_{s,CO_2}	$[-]$	3–18
Δ_0	Empirical coefficient that expresses the value of vapor pressure deficit at which $f(\Delta e)=0.5$	$[Pa]$	700–3000
	Allocation and Respiration		
ω_{grw}	Growth respiration fraction	$[-]$	0.15–0.30
r_m	Respiration rate coefficient on a $10°C$ base	$[gC\ gN^{-1}\ day^{-1}]$	0.020–0.066
N_l	Foliage carbon-nitrogen C:N mass ratio	$[gC\ gN^{-1}]$	15–42
ϵ_{al}	Tuning parameter for carbohydrate reserve allocation	$[-]$	0–1
R_{ltr}	Maximum leaf-to-root or shoot-to-root ratio	$[-]$	0.25–1.5
T_{rC}	Specific translocation rate	$[gC\ m^{-2}\ PFT\ day^{-1}]$	0.2–6
	Tissue Turnover		
d_{root}	Turnover rate of fine roots	$[day^{-1}]$	1/240−1/1500
d_{sapw}	Living sapwood to heartwood conversion rate	$[day^{-1}]$	1/365−1/2500
A_{cr}	Critical age for leaf shed	$[day^{-1}]$	50-1500
$d_{d\ max}$	Maximum turnover rate induced by drought	$[day^{-1}]$	1/30−1/600
d_{cold}	Linear coefficient for foliage loss due to cold	$[day^{-1}\ °C^{-1}]$	1/15−1/365
T_{cold}	Temperature threshold for foliage loss	$[°C]$	(−12)–(+10)
	Phenology Parameters		
$T_{s,LO}$	Prescribed temperature threshold for vegetation growth beginning	$[°C]$	
β_{LO}	Prescribed moisture stress threshold for vegetation growth beginning	$[-]$	0.7–1
$J_{Day,LO}$	Maximum Julian day for leaf onset	$[-]$	
d_{MG}	Number of days of maximum growth	$[day]$	15–40
$D_{LH,SE}$	Prescribed threshold on day length for senescence beginning	$[h]$	10–13
LAI_{min}	Minimum leaf area index at which canopy is considered to be completely defoliated	$[-]$	0.001–0.05

and bare soil fluxes to the element-scale flux values. The partition is important, since it may strongly affect the estimation of the surface water and energy fluxes.

[27] It should be noted that an explicit representation of vertical vegetation composition is not very common in climate and ecohydrological modeling with few exceptions [*Foley et al.*, 1996; *Baldocchi and Wilson*, 2001; *Ma et al.*, 2007; *Drewry et al.*, 2010a]. It is however expected to improve the simulation capabilities in environments characterized by co-existence of understory and overstory canopies (e.g., savannas, temperate forests).

4. Spatial Connections Among Basic Computational Elements

[28] The basic computational element represents a part of a hillslope. It exchanges water in the subsurface and over the surface with neighboring elements (Figure 3b). The channel network is identified using topographic attributes, such as thresholds for upstream drainage area or slope-area functions [*Montgomery and Dietrich*, 1988, 1989; *Orlandini et al.*, 2011]. Alternatively, channel locations in the model can be
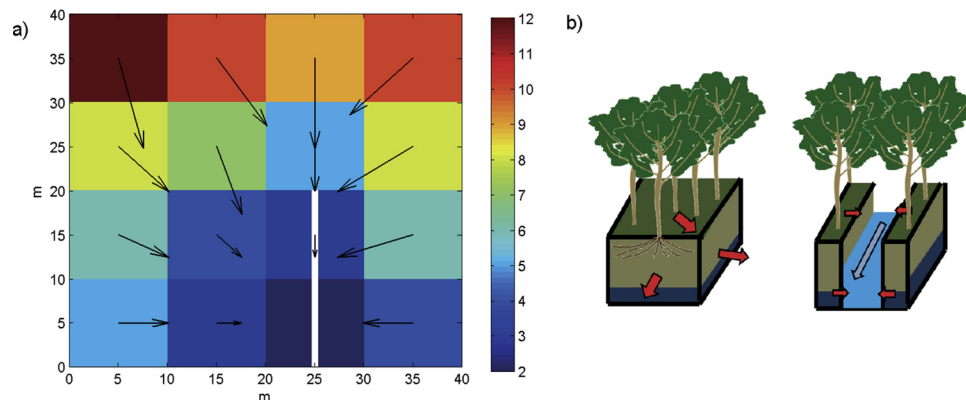
Figure 3.   A representation of topographic features and connections among basic computational elements. (a) A fragment of a Digital Elevation Model with arrows showing the flow directions and the white line representing a channel. (b) A conceptual scheme of a basic computational element with and without a subgrid channel element.

imposed explicitly on the basis of available geographic information.

[29] In T&C, channels are considered as "subgrid" domains. Specifically, channel elements are a particular type of grid cells that contain a channel reach along with a hillslope fragment (Figure 3b). In these cells, overland and channel flows may occur simultaneously. Both overland and subsurface flows are assumed to contribute to the channel streamflow. Further details are described in Sections 5.7 and 5.8.

[30] The approach used to route water mass over the surface and the subsurface domains follows the well developed concept of topographic flow directions [*O'Callaghan and Mark*, 1984; *Quinn et al.*, 1991; *Tarboton*, 1997; *Orlandini et al.*, 2003; *Nardi et al.*, 2008; *Orlandini and Moretti*, 2009; *Schwanghart and Kuhn*, 2010]. T&C has various options of approximating flow directions. For instance, a multiple direction method [*Quinn et al.*, 1991] can be used to compute directions for the subsurface domain, and the D-∞ method [*Tarboton*, 1997] for the surface (Figure 3a). When water moves into a neighboring cell, the flow window width that is assumed in the flux computation always corresponds to the length of grid square in the cardinal direction. This is an approximation for diagonal transfers as compared to other methodologies [*Quinn et al.*, 1991]. The same cell length is also used to compute the actual distance covered by flow, regardless whether the movement occurs in the diagonal or cardinal direction.

5. Model Description: Hydrology

[31] This section provides a brief description of conceptual assumptions and an overall framework of mathematical formulation of the model components, specifically, energy and water fluxes, snow dynamics, unsaturated-saturated zone interactions, and subsurface-surface flows. For a detailed description and methodological solutions, the reader is referred to the auxiliary material.

5.1. Radiative fluxes

[32] At the element scale, net radiation, $R_n [W\,m^{-2}]$, is given by the sum of absorbed shortwave, $R_{abs} [W\,m^{-2}]$, and longwave, $L_{abs} [W\,m^{-2}]$, fluxes. The sum of net radiation and heat with precipitation, Q_v, is partitioned into sensible heat, H, latent heat, λE, and ground heat, G, fluxes (Section 5.2).

5.1.1. Shortwave Radiation

[33] The total incident solar radiation is provided for the model as input partitioned into direct beam, R_{dir}, and diffuse radiation, R_{dif}. These are further partitioned into the ultraviolet-visible (UV/VIS), and the near-infrared (NIR) wavebands. Given these fluxes for a horizontal plane, the remote and local topographic effects of the simulation domain are directly accounted for and the values of R_{dir} and R_{dif} are adjusted by using such variables as sky-view factor and shadow effect [*Bertoldi et al.*, 2006a; *Fatichi*, 2010; *Fatichi et al.*, 2011].

[34] For a vegetated surface, the incident shortwave radiation propogates through *high-vegetation* canopy and then through *low-vegetation* canopy, ultimately reaching the understory ground. Radiative transfer through and absorption by two vegetation canopies is calculated by applying the two-stream approximation method [*Dickinson*, 1983; *Sellers*, 1985; *Sellers et al.*, 1996; *Dai et al.*, 2004]. When only a single vegetation layer is present, the shortwave transfer scheme reduces to the one presented in *Oleson et al.* [2004]. The transfer and absorption of *Photosynthetically Active Radiation* is calculated analogously to shortwave radiation in the ultraviolet-visible band.

[35] The overall transfer and absorption of the incoming shortwave radiation through vegetation depends on the albedos of canopy and understory surface, which may be covered by snow.

[36] The total shortwave radiation flux absorbed by a non-vegetated surface, such as bare soil, water, or snow in an open field is a function of the sky view factor and of the surface albedos. The ground albedo for bare soil and for understory ground is parameterized based on the soil surface moisture content [*Dickinson et al.*, 1993; *Oleson et al.*, 2004]. The snow albedo is a function of snow age and thermodynamic condition of snow, e.g., freezing or melting condition [*Douville et al.*, 1995; *Pederson and Winther*, 2005; *Mölders et al.*, 2008]. The albedo of water is parameterized based on solar altitude [*Bonan*, 1996].

5.1.2. Longwave Radiation

[37] Net longwave radiation, $L_{abs} [W\,m^{-2}]$, is given as the difference between the incoming longwave radiation and the outgoing longwave radiation. The incoming longwave radiation is the downward atmospheric radiation calculated from air temperature, sky view factor, clear sky emissivity, and cloudiness [*TVA*, 1972; *Idso*, 1981; *Bras*, 1990]. The outgoing radiation depends on the radiative temperature of the surface, through the Stefan-Boltzmann law.

[38] The net longwave radiation for two vegetation layers and understory ground is calculated accounting for the respective emissivities and absorptivities. In the case of a single vegetation layer, the longwave radiation absorption reduces to the scheme described in *Bonan* [1996]. For a non-vegetated surface, the net long-wave radiation depends only on the surface temperature and the surface emissivity. The presence of a snowpack alters the longwave radiation exchange as a function of snow depth which is compared to the height of low-vegetation layer (see auxiliary material).

5.1.3. Net Radiation

[39] The total net radiation, $R_n [W\,m^{-2}]$, absorbed at the element scale is a weighted sum of the net radiation absorbed by a given land cover fraction, i.e., vegetated areas, bare soil areas, water, and snow covered surface:

$$R_n = R_{n,H_v} + R_{n,L_v} + R_{n,soil} + R_{n,sno} + R_{n,wat}, \quad (1)$$

where R_{n,H_v}, R_{n,L_v} and, $R_{n,soil} [W\,m^{-2}]$ are the components denoting the total radiation absorbed by *high vegetation*, *low vegetation*, and soil ground. These terms already account for the weights of respective fractions in respective elements (auxiliary material). The absorbed

net radiation fluxes by snow and water surfaces at the element scale are $R_{n,snow}$ and $R_{n,wat}$ [$W\ m^{-2}$], respectively. The calculation of all of these quantities accounts for possible multiple PFTs within an element, and for a "masking" effect of vegetation on snow.

5.2. Soil-Vegetation-Atmosphere Mass and Heat Transfer

[40] In order to estimate sensible and latent heat fluxes between the ground surface and the atmospheric surface layer, the model employs a resistance analogy scheme [*Garratt*, 1992; *Arya*, 2001; *Brutsaert*, 2005; *Sellers et al.*, 1997]. Due to the high level of actual detail, only a generic framework used in the estimation of sensible, latent, and ground heat fluxes is described in this section. A detailed presentation can be found in the auxiliary material.

5.2.1. Sensible Heat

[41] The sensible heat flux, H [$W\ m^{-2}$], between the ground surface and the atmospheric surface layer at a reference height, z_{atm}, is a weighted sum of different land cover fractions, ϕ_i. It is assumed that the heat stored by vegetation is negligible. Therefore, sensible heat flux at the element scale is $H = \sum_{i=1}^{n_c}(\phi_i H_i)$, where H_i is sensible heat from a land cover of type i of a given element. The most general form for sensible heat flux of a vegetated or non-vegetated surface can be written as a function of the surface temperature, T_s [$°C$]:

$$H_i = f[C_{sno}]\rho_a C_p\ \frac{(T_s - T_a)}{r_{path}},\qquad(2)$$

where C_p [$J\ kg^{-1}\ K^{-1}$] is the specific heat capacity of air at a constant pressure, ρ_a [$kg\ m^{-3}$] is the air density, $f[C_{sno}]$ is a function reflecting the presence and the effect of snow, r_{path} [$s\ m^{-1}$] is a specific resistance path of the heat flux and is a function of the land cover type i and the land cover composition of the basic computational element. The prognostic radiative temperature, T_s, is considered to be homogenous within a basic element, i.e., it reflects the aggregated effect of energy partition by n_c types of land cover within the element. Further details on the form of H_i and the resistance paths can be found in the auxiliary material.

5.2.2. Latent Heat

[42] The latent heat flux, λE [$W\ m^{-2}$], or, specifically, condensation, sublimation, evaporation, and transpiration fluxes of moisture between the surface and the atmospheric surface layer are similarly calculated as the weighted sum of different land cover fractions. It is assumed that water vapor stored by vegetation is negligible. The latent heat flux at the element scale is $\lambda E = \sum_{i=1}^{n_c}(\phi_i \lambda E_i)$, where λE_i [$W\ m^{-2}$] is the latent heat from a land cover of type i. The evaporation and transpiration fluxes from different parts of a vegetated surface and from non-vegetated land cover types are estimated once the specific humidity at saturation, $q_{sat}(T_s)$ [$-$], at the prognostic surface temperature T_s is known. A general equation expressing the flux estimation is

$$E_i = f[C_{sno}]\frac{\rho_a(\alpha q_{sat}(T_s) - q_a)}{r_{path}},\qquad(3)$$

where E_i [$kg\ m^{-2}\ s^{-1}$] is a transpiration/evaporation/sublimation/condensation flux, q_a [$-$] is the specific humidity of air at the reference height. The term α [$-$] is the relative humidity at the evaporative surface, and r_{path} is a specific resistance path of the evaporative flux. All of the evaporation and transpiration terms can be limited by the effective availability of water in the soil, snowpack, and interception storage. Further details can be found in the auxiliary material.

5.2.3. Ground and Advection Heat Fluxes

[43] The flux of heat into the ground, G [$W\ m^{-2}$], is calculated with the "force-restore" method [*Deardorff*, 1978; *Hu and Islam*, 1995].

[44] The heat flux associated with precipitation, Q_v [$W\ m^{-2}$], is calculated as the energy required to convert precipitation to the prognostic surface temperature, T_s [$°C$]. When snow is present, the latter represents the temperature of snowpack [*Tarboton and Luce*, 1996; *Essery et al.*, 1999; *Williams and Tarboton*, 1999].

5.2.4. Energy Balance

[45] The prognostic temperature, T_s, is required in the estimation of heat fluxes to close the energy balance. Incoming heat with precipitation, Q_v, net radiation, R_n, sensible heat, H, latent heat, λE, and ground heat, G, are all calculated based on T_s. Neglecting the heat stored by vegetation canopy, the heat released by CO_2 fixation, and any lateral advective fluxes, the surface energy balance in the absence of snow becomes:

$$R_n(T_s) - H(T_s) - \lambda E(T_s) - G(T_s) + Q_v(T_s) = 0.\quad(4)$$

Equation (4) is highly non-linear. For instance, all of the resistance terms (see the auxiliary material) depend on T_s, and thus its solution has to be found numerically. The closure of the energy balance in presence of snow is described in Section 5.4.

[46] The assumption of a single prognostic temperature, T_s, is an important simplification adopted in T&C. This value represents a homogeneous radiative temperature of the surface in a given computational element. It is assigned to all land cover types present within an element in the absence of snow. When snow cover is present at the ground, T_s is assumed to represent the snowpack temperature, and the full energy budget of snow-free vegetation surfaces is not explicitly resolved. Specifically, this assumption implies that snow-free vegetation emits sensible heat flux in the amount equivalent to the absorbed net radiation, and that transpiration flux from vegetated surface is considered to be negligible. Justifications of the above assumptions can be found in the auxiliary material.

5.2.5. Energy and Mass Transfer Resistances

[47] The parameterization of vertical heat fluxes is based on an analogy with the Ohm's law. A number of serial and parallel resistances are used to mediate the transfer of heat and water vapor between the land

surface (vegetation, bare soil, snow, and water) and the atmospheric surface layer. Five different types of resistance are accounted for: the aerodynamic resistance, r_a, the leaf boundary layer resistance, r_b, the undercanopy resistance, r_a', the soil resistance, r_{soil}, and the stomatal resistance r_s. The resistances have the dimensions of inverse of velocity [$s\ m^{-1}$] and depend on many factors including surface roughness (e.g., the canopy structure and leaf dimensions), wind speed, surface temperature, and atmospheric stability, to name a few. A brief summary of each resistance type is provided below.

[48] The aerodynamic resistance to heat and water vapor transfer between the major sinks of heat/vapor and the reference height, r_a, can be calculated in two ways in T&C: either by applying the complete Monin-Obukhov similarity theory [*Monin and Obukhov*, 1954; *Louis*, 1979; *Abdella and McFarlane*, 1996; *van den Hurk and Holtslag*, 1997] or by using a simplified parameterization [*Mascart et al.*, 1995; *Noilhan and Mafhouf*, 1996].

[49] The undercanopy resistance, r_a' [sm^{-1}], i.e., the aerodynamic resistance between the understory ground surface and the level of source of heat/vapor in vegetation layer or between the two levels of sources in vegetation (when two vegetation layers are present) is parameterized as in *Zeng et al.* [2005] and *Sakaguchi and Zeng* [2009].

[50] The resistance to exchanges of water vapor, carbon dioxide, and heat exerted by a thin layer of air between the leaf surfaces and the surrounding environment, r_b [$s\ m^{-1}$], is modeled as a function of leaf width and flow characteristics [*Choudhury and Monteith*, 1988; *Shuttleworth and Gurney*, 1990].

[51] The resistance to bare ground evaporation is parameterized using the "β method", as proposed by *Sellers et al.* [1992, 1996], and *Oleson et al.* [2008].

[52] The approach employed by T&C for estimating r_s is outlined in Section 5.3.

5.3. Approach to Stomatal and Photosynthesis Modeling

[53] A framework for estimation of the stomatal resistance, r_s [sm^{-1}], the net assimilation rate, A_{nC} [$\mu mol\ CO_2\ s^{-1}\ m^{-2}$], and the dark respiration R_{dC} [$\mu mol\ CO_2\ s^{-1}\ m^{-2}$] is briefly outlined in this section. These quantities are calculated using a coupled model of photosynthesis and stomatal resistance.

5.3.1. Leaf to Canopy Scaling

[54] The fluxes of energy, water, and CO_2 for a vegetated surface need to be scaled from leaf to the canopy scale because of several existing non-linear interactions [*de Pury and Farquhar*, 1997; *Wang and Leuning*, 1998; *Dai et al.*, 2004]. A "big-leaf" approach is used in T&C to model the canopy-scale mass and energy fluxes [*Farquhar*, 1989; *Sellers et al.*, 1996; *Bonan*, 1996; *Friend et al.*, 1997; *Dickinson et al.*, 1998; *Oleson et al.*, 2004]. The big-leaf model requires a conceptualization of the vertical profile of photosynthetic properties in the plant. Specifically, the canopy nitrogen profile is assumed to decay exponentially, controlled by a factor, K_N [$-$]. Since the maximum photosynthetic capacity has been shown to depend

linearly on leaf nitrogen content [*Schulze et al.*, 1994; *White et al.*, 2000; *Reich et al.*, 1997; *Wright et al.*, 2004], the assumed distribution of nitrogen is used to scale relevant photosynthetic properties, such as the maximum Rubisco capacity and the maximum electron transport capacity (see the auxiliary material for details).

5.3.2. Stomatal Resistance

[55] A biochemical model describing the coupling between photosynthesis and stomatal resistance is used in T&C. Simplifications are introduced in order to reduce the computational effort and to account for the limitations imposed by a single prognostic temperature. Details of the biochemical model of photosynthesis are provided in the auxiliary material.

[56] The aperture of stomata has been experimentally shown to be related to net assimilation rate of CO_2, A_{nC}, environmental vapor pressure deficit, Δe [Pa], and intercellular CO_2 concentration, c_i [Pa] [*Ball et al.*, 1987; *Leuning*, 1995]. It is important to note that all empirical stomatal conductance relationships give a linear dependence between the net assimilation rate A_{nC} and the stomatal conductance g_{s,CO_2}. Several empirical equations to calculate stomatal conductance have been proposed in literature [*Ball et al.*, 1987; *Tardieu and Davies*, 1993; *Dewar*, 2002; *Tuzet et al.*, 2003]; the parameterization proposed by *Leuning* [1990, 1995] is used in T&C:

$$g_{s,CO_2} = g_{0,CO_2} + a\frac{A_{nC}}{(c_i - \Gamma^*)}f(\Delta e)\ P_{atm}, \qquad (5)$$

where g_{s,CO_2} [$\mu mol\ CO_2\ m^{-2}\ leaf\ s^{-1}$] is the stomatal conductance, $g_{s,CO_2} = 1/r_{s,co_2}$, a [$-$] is an empirical parameter, Γ^* [Pa] is the CO_2 compensation point, P_{atm} [Pa] is the atmospheric pressure, and g_{0,CO_2} [$\mu mol\ CO_2\ m^{-2}\ leaf\ s^{-1}$] is the cuticular conductance or minimum stomatal conductance when $A_{nC} \leq 0$. The function of sensitivity to atmospheric vapor pressure deficit is $f(\Delta e) = (1 + \Delta e/\Delta_0)^{-1}$, where Δe [Pa] is the vapor pressure deficit calculated with T_a, and Δ_0 [Pa] is an empirical coefficient that expresses vapor pressure deficit at which $f(\Delta e = \Delta_0) = 0.5$. Equation (5) takes into account the correction of *Tuzet et al.* [2003], where the CO_2 concentration at the leaf surface c_s [Pa] is replaced with the leaf internal concentration c_i [Pa], which better agrees with the observed stomatal response [*Mott*, 1988; *Assmann*, 1999]. The photosynthesis rates and stomatal conductance thus depend on leaf internal partial pressure of CO_2, c_i [Pa] that, a priori, is unknown (see the auxiliary material). An iterative procedure is thus required to estimate c_i, which is formulated as a problem of finding the roots of a non-linear equation, once the resistance scheme between the leaf interior and the atmosphere is accounted for.

5.4. Snow Hydrology

[57] An inclusion of a snow-hydrology component in an ecohydrological model permits the investigation of interactions between snow accumulation and vegetation, accounting for snow interception and changes in

albedo and net radiation partition. These processes deserve a special attention in the study of hydrology-vegetation linkages and their modeling is an active field of research [*Pomeroy et al.*, 1998; *Liston et al.*, 2002; *Strack et al.*, 2004; *Jost et al.*, 2007; *Veatch et al.*, 2009; *Molotch et al.*, 2009; *Essery et al.*, 2009; *Bewley et al.*, 2010; *Ellis et al.*, 2010].

[58] In the presented model, snowpack formation and melt are modeled with an approach based on thermodynamics governing the snowpack evolution [*Wigmosta et al.*, 1994; *Douville et al.*, 1995; *Essery et al.*, 1999; *Belair et al.*, 2003]. The snow hydrology module includes a single snow layer in order to avoid large computational efforts required by complex snowpack multi-layer models [*Marks et al.*, 1998; *Bartelt and Lehning*, 2002].

[59] The incoming precipitation is partitioned between rain and snow as a function of air temperature [*Wigmosta et al.*, 1994; *Tarboton and Luce*, 1996]. Two different storages of snow are considered: snow layer at the ground, with the corresponding snow water equivalent, S_{WE} [*mm*], and the intercepted snow in the *high-vegetation* layer, with the snow water equivalent, $In_{S_{WE}}$ [*mm*]. Since only a single prognostic surface temperature T_s is computed for any given computational element, the two storages are combined to compute the energy balance and assumed to be at the same temperature. The eventual snowmelt, S_m, is partitioned between snowmelt in the snowpack at the ground, S_{m1} [*mm*], and snowmelt in the intercepted snowpack, S_{m2} [*mm*].

5.4.1. Snow Energy Balance

[60] The basic theory underlying all physically-based point snowmelt models consists in balancing the energy budget for the snowpack and converting the excess energy into snowpack temperature change, metamorphism, or melt [*Williams and Tarboton*, 1999].

[61] The net energy flux input to the snowpack, dQ [*W* m^{-2}], is calculated by considering all significant sources of incoming and outgoing heat [*Anderson*, 1968; *Bras*, 1990; *Wigmosta et al.*, 1994; *Dingman*, 1994; *Tarboton and Luce*, 1996; *Williams and Tarboton*, 1999; *Liston and Elder*, 2006]:

$$dQ(T_s) = R_n(T_s) + Q_v(T_s) + Q_{fm}(T_s) - H(T_s) -$$
$$\lambda E(T_s) - G(T_s), \qquad (6)$$

where R_n [*W* m^{-2}] is the net radiation energy absorbed by snow, Q_v [*W* m^{-2}] is the incoming heat with precipitation, G [*W* m^{-2}] is the ground heat flux into the soil below snowpack layer, H [*W* m^{-2}] is the sensible heat flux from snow, λE [*W* m^{-2}] is the latent heat flux from snow and Q_{fm} [*W* m^{-2}] is the heat release from melting (negative) or freezing (positive) of liquid water held by snow.

5.4.2. Snow Mass Balance

[62] The ground snowpack mass balance S_{WE} [*mm*] is based on the following relationships:

$$S_{WE}^b(t) = S_{WE}(t - dt) + P_{r,us}(t) - E_{sno}(t)dt, \qquad (7)$$

$$S_{WE}(t) = S_{WE}^b(t) - S_{m1}(t), \qquad (8)$$

where S_{WE}^b [*mm*] is the snow water equivalent of ground snow layer before accounting for melting, $P_{r,us}$ [*mm*] is snow precipitation that reaches the ground, E_{sno} [*mm* h^{-1}] is the evaporation-sublimation from the snowpack and dt [*h*] is the time step. The term $P_{r,us}$ is given by the total snow precipitated in the area in addition to unloading from intercepted snow, $U_{In_{S_{WE}}}$ [*mm*], less the newly intercepted snow, $In_{S_{WE}}^N$ [*mm*]. For further details, the reader is referred to *Fatichi* [2010].

[63] All of the quantities in equation (6) are functions of unknown surface temperature T_s. Further, T_s depends on the snow mass balance (equations (7) and (8)), since it influences snowmelt and liquid water content on the snowpack. An iterative numerical solution has been developed to solve for T_s that satisfies the energy and mass balances.

5.4.3. Canopy Interception of Snow

[64] In T&C, only *high-vegetation* layer (H_v) is parameterized to have a storage of intercepted snow. A single value of intercepted snow water equivalent, $In_{S_{WE}}$ [*mm*], is considered for any given element and it represents the average of intercepted snow among different *PFTs* that can be present within a basic computational element. The *low-vegetation* layer does not have storage for snow interception. When unloaded from the high-vegetation layer or when it directly falls on the *low-vegetation* layer, snow is assumed to increment the ground snow layer with a corresponding contribution added to S_{WE}. The presence of snow on the ground is assumed to completely hide the *low-vegetation* layer.

[65] *Hedstrom and Pomeroy* [1998] provide a physically-based formulation of snow interception, where the intercepted snow mass, $In_{S_{WE}}$, is related to snowfall characteristics, leaf area index, tree species, canopy density, air temperature, and wind speed [*Hedstrom and Pomeroy*, 1998; *Pomeroy et al.*, 1998, 2002; *Gelfan et al.*, 2004]. Further adaptations presented by *Gelfan et al.* [2004], *Lee and Mahrt* [2004], and *Liston and Elder* [2006] are also accounted for and implemented in T&C. A detailed description of the implementation details can be found in *Fatichi* [2010].

[66] The parameterization of snowpack water content, snow depth, snow density, and surface roughness change due to snow [*Verseghy*, 1991; *Douville et al.*, 1995; *Wigmosta et al.*, 1994; *Belair et al.*, 2003; *Strack et al.*, 2004] are discussed in the auxiliary material.

5.5. Canopy Interception of Liquid Flux

[67] Interception of liquid precipitation can be partitioned into canopy and forest floor interception storages. Canopy interception by *high-vegetation* and *low-vegetation* are simulated. The scheme neglects forest floor interception, as well as the storage of water in ponds, puddles, and surface microdepressions [*Kamphorst et al.*, 2000; *Gerrits et al.*, 2007].

[68] Precipitation is subdivided into the flux intercepted by canopy, throughfall flux, and canopy drainage

[*Mahfouf and Jacquemin*, 1989; *Dickinson et al.*, 1993; *Ramrez and Senarath*, 2000]. Canopy interception, *In* [*mm*], is estimated using a Rutter-type model for each *Crown Area*, C_{crown}, and separately for the two vegetation layers [*Rutter et al.*, 1971, 1975].

5.6. Vadose Zone Dynamics

[69] Vadose zone dynamics exert an important control on the hydrological cycle. The soil moisture profile with depth z, $\theta(z)$, directly influences processes such as infiltration, storm runoff, lateral subsurface flow, and groundwater aquifer recharge. Furthermore, the soil moisture distribution directly or indirectly affects (mainly through the temperature T_s) all of the energy fluxes.

[70] The influx of water, q_{ins} [*mm* h^{-1}], at the soil surface can be a sum of several components: direct rainfall on nonvegetated areas, throughfall for two vegetation layers, water released from the snowpack, drainage of intercepted water, and dew. An external flux, the runon, q_{runon} [*mm* h^{-1}], can be considered as another possible component of the flux q_{ins}. Runon for a given element is estimated as the sum of surface runoff produced in neighboring elements that contribute their flow to a considered element following

predefined drainage pattern. Runon may become important in semi-arid environments, where discontinuous and intermittent patterns of surface flow create conditions for downstream re-infiltration of a significant portion of runoff [*Howes and Abrahams*, 2003]. Depending on the magnitude of q_{ins} and antecedent soil moisture conditions, the flux may either infiltrate or be excluded, partially or entirely, as surface runoff [*Panday and Huyakorn*, 2004; *Brutsaert*, 2005; *Kollet and Maxwell*, 2006; *Maxwell and Kollet*, 2008].

5.6.1. Formulation

[71] The Richards equation is solved numerically in its one-dimensional formulation using a finite volume approach with, an adaptation of the ''method of lines'' [*Lee et al.*, 2004]. In short, in order to evaluate the soil moisture contents, θ_i [$m^3 m^{-3}$], the Richards equation, i.e., the partial differential equation, is reduced to a system of ordinary differential equations. The soil column is subdivided into $i=1,\ldots,n_s$ layers (Figure 4) and each layer i is characterized by the depth from the surface to a layer upper boundary, $Z_{s,i}$ [*mm*], the layer thickness, $d_{z,i}$ [*mm*], and a distance between the layer center and the center of preceding layer, $D_{z,i}$ [*mm*]. The resultant ordinary differ-
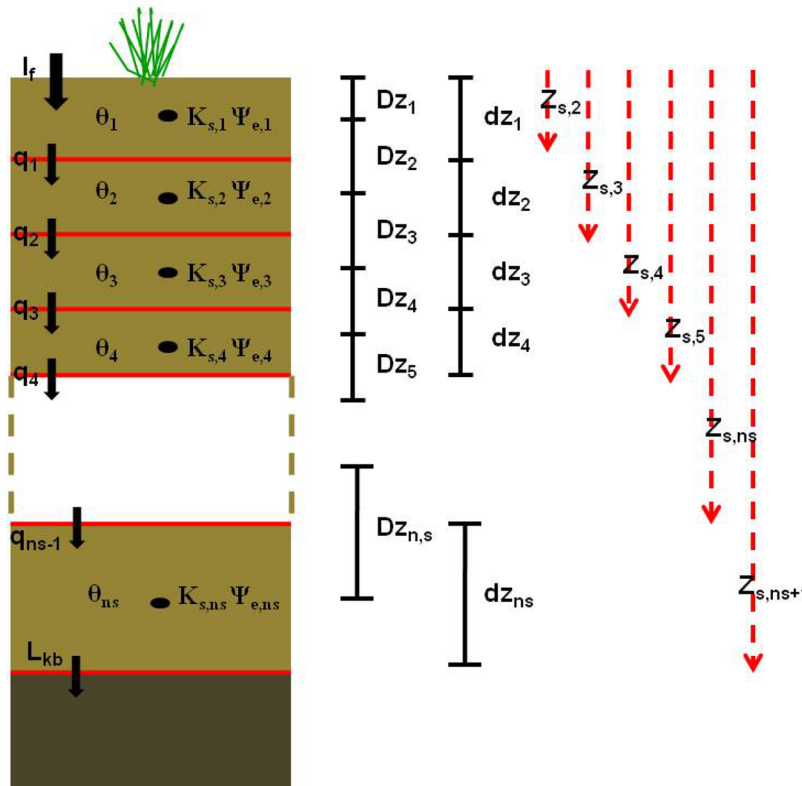
Figure 4. A graphical scheme illustrating a soil column representation and the principal variables used in the computation of subsurface water dynamics. The subscript i identifies a soil layer. The term $\Psi_{e,i}$ [*mm*] is the water potential at the air entry at the center of the layer, $K_{s,i}$ [*mm* h^{-1}] is the saturated conductivity at the center of layer, L_{kb} [*mm* h^{-1}] is the bottom leakage flow. The soil water content is θ_i [−], q_i [*mm* h^{-1}] is the vertical outflow from layer i, $Z_{s,i}$ [*mm*] is the depth from the surface to the layer upper boundary, $d_{z,i}$ [*mm*] is the layer thickness, and $D_{z,i}$ [*mm*] is a positive distance between the layer center and the preceding layer center. Note that the first value of Z_s is always zero, corresponding to the surface. Typically, between 8 and 20 layers are used with a coarser mesh resolution at greater depths for computational efficiency.

ential equations are of the following general form:

$$d_{z,i} \frac{d\theta_i}{dt} = q_{i-1} - q_i - \sum_{j=1}^{n_c} T_{H_v,j}\, r_{H_v,i,j} - \sum_{j=1}^{n_c} T_{L_v,j}\, r_{L_v,i,j} -$$

$$\sum_{j=1}^{n_c} E_{g,j} - E_{bare} + Q_{l,in,i} - Q_{l,out,i}, \qquad (9)$$

where $q_i\,[mm\,h^{-1}]$ is the vertical outflow from a layer i, the terms with the j index quantify moisture sinks in vegetation patches, and n_c is the number of different *Crown Areas* in the present element. The sinks at the soil surface and in the root zone are due to evapotranspiration process. They can be subdivided into the following components: evaporation from bare soil, $E_{bare}\,[mm\,h^{-1}]$, evaporation from the soil under canopy, $E_g\,[mm\,h^{-1}]$, and transpiration from high- and low-vegetation layers, T_{H_v}, and $T_{L_v}\,[mm\,h^{-1}]$. The fluxes E_g and E_{bare} are assumed to have access to moisture only in the first soil layer. The treatment of the fraction of root biomass contained in a given soil layer, $r_i\,[-]$, is described in the auxiliary material. The lateral outflows, $Q_{l,out,i}\,[mm\,h^{-1}]$, are calculated according to the soil moisture content and an approximation of lateral head gradient (see Section 5.7). The incoming lateral subsurface fluxes, $Q_{l,in,i}\,[mm\,h^{-1}]$, are the sum of subsurface water fluxes originating in neighboring elements. The vertical outflow from a layer i is

$$q_i = \overline{K_{v,i}} \left(1 + \frac{\Psi_i - \Psi_{i+1}}{Dz_{i+1}} \right), \qquad (10)$$

where $\overline{K_{v,i}}\,[mm\,h^{-1}]$ is the unsaturated hydraulic conductivity averaged between the layers i and $i+1$, and $\Psi_i\,[mm]$ is the soil water potential of the layer i. In heterogenous soil conditions, the soil hydraulic properties at a given depth z_i are also a function of the layer depth.

[72] Note that the number of computed fluxes q_i is n_s-1 because the inflow to the first soil layer is calculated as infiltration, $I_f\,[mm\,h^{-1}]$, and the vertical outflow from the deepest soil layer is considered as leakage to the underlying bedrock, L_{kb} (Section 5.7).

5.6.2. Infiltration Excess Runoff

[73] The infiltration term in T&C is computed by using a technique that first imposes a "hypothetical" Dirichlet boundary condition at the soil surface, under which the surface soil water potential is equal to zero. This is done in order to estimate the upper limit for infiltration flux, i.e., the infiltration capacity, $I_f^C\,[mm\,h^{-1}]$. When the total water influx q_{ins} is less than I_f^C, the situation corresponds to the Neumann-type flux boundary condition and the flux enters the soil. Once ponding occurs (under which condition q_{ins} is higher than I_f^C), the condition corresponds to a Dirichlet-type boundary condition, with the soil water potential assigned to be zero or positive at the soil surface (i.e., the saturation condition with the pond depth estimated as a function of q_{ins}).

[74] Infiltration excess runoff, also called the *Hortonian* runoff, is calculated as the difference between the water influx to soil, q_{ins}, and the actual infiltration rate $I_f\,[mm\,h^{-1}]$, $R_H = q_{ins} - I_f\,[mm\,h^{-1}]$. The actual infiltration rate is $I_f = \min(q_{ins}, I_f^C)\,[mm\,h^{-1}]$, where "min" is the minimum operator.

5.6.3. Saturation Excess Runoff

[75] A soil layer i of the soil column becomes saturated, once it reaches the soil saturation content $\theta_{sat}\,[-]$. If this occurs when inflow to the layer i is larger than the outflow, a saturated zone within the soil column is formed with the water table depth located at $Z_{wt}\,[mm]$, where Z_{wt} represents the depth of the shallowest saturated layer. The model assumes that a surplus water from the layer i is transferred to upper layers; if the entire soil column is saturated, water exfiltrates to the surface through the top layer. Runoff generated in this fashion is called the saturation excess runoff, $R_D\,[mm\,h^{-1}]$.

5.6.4. Soil Properties

[76] Soil texture is one of the key variables in the coupled dynamics between climate, soil, and vegetation [*Fernandez-Illescas et al.*, 2001; *Ivanov*, 2006]. T&C can use two parameterizations for water retention, $\Psi(\theta)$, and unsaturated conductivity, $K_v(\theta)$, curves, specifically, the *vanGenuchten* [1980] and *Saxton and Rawls* [2006] parameterizations (see also *Fatichi* [2010] for details). An evaluation of the parameters used to characterize the water retention and the unsaturated conductivity curves can be realized with pedotransfer functions [*Saxton and Rawls*, 2006; *Vereecken et al.*, 2010].

[77] Possible heterogeneities in the soil hydraulic conductivity are accounted for with an "anisotropy" factor, a_r. The factor, $a_r = K_h/K_v\,[-]$, is defined as the ratio between the hydraulic conductivity in the directions parallel to the slope, K_h, and the hydraulic conductivity normal to the slope, K_v. This is similar to the approach of *Garrote and Bras* [1995]. Typically, the value of a_r is larger than 1. The value of K_h can be an order of magnitude larger than K_v.

5.6.5. Surface Sealing

[78] Surface sealing and soil crust formation can be accounted for in the T&C model. This process decreases the infiltration rate, reduces water available to plants in the root zone, diminishes the natural recharge of aquifers, and increases runoff and soil erosion [*Mualem et al.*, 1990; *Mualem and Assouline*, 1989; *Assouline and Mualem*, 1997, 2001; *Assouline*, 2004]. Therefore, soil sealing effects can be of paramount importance in ecohydrological modeling, especially when arid and semiarid environments with large portions of bare soil are investigated. However, given the difficult parameterization of this process (see the auxiliary material), the surface sealing component is only enabled for specific applications, typically for environments where bare soil is the dominant fraction of land cover.

5.7. Subsurface Flow

[79] Water transferred sideways from the soil column in a given element, $Q_{l,out}\,[mm\,h^{-1}]$, represents lateral subsurface flow. It is assumed in T&C that the slope of the hydraulic head is parallel to the soil surface, i.e., the

assumption that is commonly made in the topographic subsurface routing methods [*Beven and Kirkby*, 1979; *Sivapalan et al.*, 1987; *Beven and Freer*, 2001; *Ciarapica and Todini*, 2002]. The assumption validity is violated in shallow terrains (e.g., floodplain), especially when a portion or the entire soil column becomes saturated. A hydraulic head gradient formulation would be preferable [*Wigmosta and Lettenmaier*, 1999; *Panday and Huyakorn*, 2004; *Kollet and Maxwell*, 2008] and is regarded as a potential future improvement of the model. The lateral flow from a layer i, $Q_{l,out,i}$, moves along a pre-defined drainage flow direction(s) into the neighboring element(s):

$$Q_{l,out,i} = \frac{T_{r,i} \, \sin \beta_T}{a_T} \, , \qquad (11)$$

where β_T [*rad*] is the maximum surface slope of an element, a_T [*mm*] is the element area per unit contour length that drains through the location [*Quinn et al.*, 1995; *Sivapalan et al.*, 1987], and $T_{r,i}$ [$mm \, h^{-1}$] is the total transmissivity of the layer i. The total lateral subsurface flow from an element, $Q_{l,out}$, [$mm \, h^{-1}$], is calculated by integrating equation (11) over n_s layers. When dealing with a cell containing a channel element, the subsurface flow, $Q_{l,out}$, is added to channel flow of that grid cell. In this unidirectional operation, the effect of seepage flow is mimicked.

[80] Soil-bedrock leakage flow has been recently regarded as an important process of subsurface dynamics [*Weiler and McDonnell*, 2004; *Tromp-van Meerveld and Weiler*, 2008]. According to Figure 4, the last layer of the soil column is drained through the bottom, resulting in leakage flow, L_{kb} [$mm \, h^{-1}$]. This term represents percolation flux from the soil column (i.e., the regolith) to the bedrock. This flux is considered to be equal to the conductivity of bedrock, $L_{kb}=K_{bot}$ [$mm \, h^{-1}$], when the last n_s-th layer of soil is saturated. No unsaturated flow to the bedrock is assumed. Another possible condition, $K_{bot}=0$, implies an impermeable bedrock, which precludes recharge to deeper aquifers. A free-gravitational drainage condition can also be assumed in T&C, as another type of the bottom boundary condition.

[81] Note further that non-zero flow, L_{kb}, provides a recharge to a deep aquifer. The latter represents a reservoir with a long residence time and can be conceptualized as a lumped component at the watershed scale. The deep aquifer can return a baseflow flux, Q_{sub} [$mm^3 \, h^{-1}$], according to a reservoir scheme (see the auxiliary material) that distributes the flow throughout the watershed stream network.

5.8. Surface Water Dynamics

[82] The numerical scheme adopted for representing surface flow in T&C is a function of topographic representation of the domain (Sections 3 and 4). The runoff depth, R_{tot} [mm], in a given computational element is the sum of infiltration excess runoff, R_H [$mm \, h^{-1}$], and saturation excess runoff, R_D [$mm \, h^{-1}$]. The

flow depth of locally produced runoff, y [mm], is then approximated with the assumption of a sheet flow, i.e., for overland flow, $y=R_{tot}$. Channel is conceptualized as a sub-grid element with the rectangular cross-section of width w_{ch} [m]. The width w_{ch} is parameterized as a function of the upstream contributing area according to regional geomorphological relationships [*Orlandini*, 2002; *Camporese et al.*, 2010]. A cell containing a channel area can have both overland and channel flow components. Channels are assumed to both receive subsurface flow (see Section 5.7) and overland flow. The water depth in the channel is $y_{ch}=R_{ch} \, dx/w_{ch}$, where dx [m] is the grid cell size and R_{ch} [mm] is the runoff in the channel, expressed per unit of cell area.

[83] Surface and channel flows are successively routed using the kinematic wave approach, i.e., assuming the momentum equation $S_{fl}=\sin \beta_T$, where S_{fl} [$-$] is the energy gradient and β_T [rad] is the slope of the element [*Chow*, 1988; *Bras*, 1990; *Chanson*, 2004; *Brutsaert*, 2005]. The water surface is therefore assumed to be parallel to the cell bed at a given location. Further, assuming locally uniform flow and the Manning equation as the flow depth-discharge relationship, it is possible to calculate the overland and channel flow velocities U and U_{ch} [$m \, s^{-1}$] and, consequently, the respective time t_R and t_{ch} [s] needed to move water from a computational element to downstream element(s) [*Kollet and Maxwell*, 2006]: $U_{ch}=n_{ch}^{-1} R_{hy}^{2/3} S_{fl}^{1/2}$, where $R_{hy} \approx y_{ch}$ [m] is the hydraulic radius approximated with the flow depth, and n_{ch} [$s \, m^{-1/3}$] is the channel Manning's coefficient that characterizes river bed roughness. Consequently, the routing time is $t_{ch}= dx \, n_{ch} \, y^{-2/3} \sin \beta_T^{-1/2}$. Equivalent equations can be written for overland flow routing. The distance between the centers of two cells is always assumed to be equal to the cell size, dx. The runoff depths, R_{ch}, (or R_{tot}) [mm] present at any time in a given element are thus routed according to the time, t_{ch}, (or t_R), following the flow directions calculated from the topography (Sections 3 and 4).

[84] At the end of a given time step, a fraction of the produced runoff R_{tot} may remain in a hillslope element. At a successive time step, this runoff fraction can be re-infiltrated as runon, q_{runon} [$mm \, h^{-1}$] (Section 5.6). Finally, the rate at which overland and channel flows leave the domain or pass trough a specific location is the sum of overland flow and channel discharge, $Q=\overrightarrow{R_{tot}}/dt$ [$mm \, h^{-1}$] and $Q_{ch} = \overrightarrow{R_{ch}}/dt$ [$mm \, h^{-1}$], where $\overrightarrow{R_{tot}}$ and $\overrightarrow{R_{ch}}$ [mm] represent the routed fractions of R_{tot} and R_{ch}. In order to respect the Courant condition [*Chanson*, 2004; *Martin and Gorelick*, 2005], a fine time step must be used to route the water flow across the domain. The present version of T&C adopts a 2 s time step for channel flow and 30 s for overland flow. Note that runoff generation is still computed at the hourly time scale, which thus assumes constant production rate over that time interval (Section 5.6).

6. Model Description: Vegetation Dynamics

[85] The processes affecting the carbon balance of vegetation are outlined in this section. These include

net primary production, plant respiration, carbon allocation, translocation, and tissue turnover.

[86] Plant carbon dynamics are tracked through the time evolution of carbon pools. They store carbon that is gained as a result of photosynthetic activity. Carbon can be used for maintenance, growth, and reproduction and is lost in the process of respiration and tissue turnover. Four carbon pools for each PFT are simulated in T&C. These are the green aboveground biomass, C_{leaf} [$gC\ m^{-2}\ PFT$], living sapwood (woody plants only), C_{sapw} [$gC\ m^{-2}\ PFT$], fine roots, C_{root} [$gC\ m^{-2}\ PFT$], and carbohydrate reserve, C_{hydr} [$gC\ m^{-2}\ PFT$]. The latter term represents a fraction of labile carbon in plants, i.e., non-structural carbohydrates (glucose, fructose and sucrose, starch), lipids, and sugar alcohols [*Hoch et al.*, 2003; *Gough et al.*, 2009]. Two additional carbon pools are implicitly considered but their dynamics are not tracked explicitly in this version of T&C. They are flower and fruit, C_{fifr} [$gC\ m^{-2}\ PFT$], and heartwood, C_{heaw} [$gC\ m^{-2}\ PFT$], carbon pools. The former takes into account the reproduction cost of a plant; the latter accounts for the death of living sapwood and its conversion into structural wood in the trunk and coarse roots.

[87] Vegetation structure evolves dynamically since carbon in the different pools varies responding to environmental conditions, stresses, seasonality, etc. These dynamics directly influence vegetation attributes, such as the leaf and stem areas, canopy height, root profile, and leaf dimension. Although theoretically all of the described attributes of vegetation are time-varying, only *LAI* dynamics are explicitly formulated in this version of the model. In each *PFT*, *LAI* [$m^2\ leaf\ area\ m^{-2}\ PFT\ area$], is related to the green aboveground biomass carbon pool as $LAI = C_{leaf}S_{LAI}$, where S_{LAI} [$m^2\ LAI\ gC^{-1}$] is the specific leaf area of biomass, which is a *PFT*-dependent parameter. Vegetation models are quite sensitive to the values of S_{LAI}, since it represents the ability of plants to invest in new photosynthetic capacity; S_{LAI} generally increases with photosynthetic capacity and leaf nitrogen content and decreases with the leaf life span [*Schulze et al.*, 1994; *Reich et al.*, 1997; *Wright et al.*, 2004].

[88] The nutrient dynamics are neglected and the corresponding pools are not currently tracked. The water supply limitation is considered to be the most important factor in plant stress [*Rodriguez-Iturbe*, 2000; *Rodriguez-Iturbe et al.*, 2001; *Laio et al.*, 2001; *Porporato et al.*, 2001; *Eagleson*, 2002; *Rodriguez-Iturbe and Porporato*, 2004]. This assumption is a rationale for many ecohydrological studies in arid and semi-arid environments. The validity of such an assumption in water abundant ecosystems is questionable [*Rodriguez-Iturbe et al.*, 2001; *Mackay*, 2001; *Dickinson et al.*, 2002; *Eagleson*, 2002; *Rodriguez-Iturbe and Porporato*, 2004], even though the nutrient cycle is still mediated by water availability [*Porporato et al.*, 2003; *Tague and Band*, 2004; *Arain et al.*, 2006; *Manzoni and Porporato*, 2009].

6.1. Net Primary Production and Plant Respiration

[89] The Net Primary Production, *NPP* [$gC\ m^{-2}\ PFT\ day^{-1}$], is defined as the gross plant photosynthesis, or

Gross Primary Production, *GPP* [$gC\ m^{-2}\ PFT\ day^{-1}$], less autotrophic respiration, R_A [$gC\ m^{-2}\ PFT\ day^{-1}$] [*Ruimy et al.*, 1996; *Knorr*, 2000; *Arora*, 2002; *Sitch et al.*, 2003; *Levis et al.*, 2004; *Krinner et al.*, 2005]:

$$NPP = GPP - R_A, \tag{12}$$

$$GPP = \kappa(A_{nC} + R_{dC}), \tag{13}$$

where $\kappa = 1.0368$ [$gCs\ \mu mol\ CO_2^{-1}\ day^{-1}$] is a unit conversion factor. Vegetation autotrophic respiration, R_A, is estimated as the sum of maintenance respiration, R_m, and growth respiration, R_g [$gC\ m^{-2}\ PFT\ day^{-1}$], rates:

$$R_A = R_m + R_g, \tag{14}$$

$$R_m = R_{mF} + R_{mS} + R_{mR} + R_{mH}, \tag{15}$$

$$R_g = \max\left[0, \omega_{grw}(GPP - R_m)\right], \tag{16}$$

where ω_{grw} [$-$] is the growth respiration fraction, R_{mS}, R_{mR}, and R_{mH} [$gC\ m^{-2}\ PFT\ day^{-1}$] are the maintenance respiration rates for living sapwood, fine roots, and carbohydrate reserves, respectively, and $R_{mF} = \kappa R_{dC}$ [$gC\ m^{-2}\ PFT\ day^{-1}$] is the rate of foliage maintenance respiration. The maintenance respiration R_m is subdivided among living plant compartments [*Thornley*, 1970; *McCree*, 1970; *Ryan*, 1991; *LeRoux et al.*, 2001]. It is calculated as a function of temperature and biomass, according to the prescribed nitrogen to carbon ratio of each tissue [*Ryan*, 1991; *Ruimy et al.*, 1996; *Sitch et al.*, 2003; *Reich et al.*, 1998; *Krinner et al.*, 2005; *Reich et al.*, 2006]. For a detailed description of relevant parameterizations, the reader is referred to the auxiliary material and *Fatichi* [2010].

6.2. Carbon Allocation and Translocation

[90] Carbon allocation in T&C is treated following *Friedlingstein et al.* [1998] and *Krinner et al.* [2005], who provide an allocation scheme that responds dynamically to temporal variability of resources. The use of a dynamic, stress-dependent scheme permits more flexible patterns of carbon redistribution [*Arora and Boer*, 2005; *Ivanov et al.*, 2008]. The basic hypothesis in the model of *Friedlingstein et al.* [1998] is that a plant will allocate carbon to different compartments in response to external limitations: water, light, and nitrogen availability. The allocation is also made dependent on the phenological state that a plant experiences; for instance, carbon is entirely allocated to leaves during the maximum growth state and predominantly to carbohydrate reserves during senescence (Section 6.5). Carbon allocation is also regulated by allometric constraints. These represent relationships among different structural compartments that have been observed experimentally [*Lüdeke et al.*, 1994; *Kozlowski and Pallardy*, 1997;

Friend et al., 1997; *Bonan et al.*, 2003; *Hoch et al.*, 2003; *Körner*, 2003; *Levis et al.*, 2004; *Arora and Boer*, 2005; *Krinner et al.*, 2005; *Ivanov et al.*, 2008; *Deckmym et al.*, 2008; *Gough et al.*, 2009; *Millard and Grelet*, 2010]. T&C uses two fundamental allometric constraints: a minimum root:shoot ratio, i.e., the ratio of fine root carbon to foliage carbon; and an upper limit for the storage of carbohydrate reserve. The latter limit is parameterized as a fraction of living sapwood biomass or fine root biomass (for herbaceous species).

[91] First, constraint-free allocations are estimated. A subsequent procedure in T&C modifies these allocations, so that allometric relationships are satisfied. The final procedure partitions the photosynthate to pools with allocation fractions corresponding to green aboveground biomass, f_l, living sapwood, f_s, fine roots, f_r, carbohydrate reserves, f_h, and fruit and flowers, f_f. Since the fruit and flower carbon pool is not tracked, the carbon allocated through f_f is simply subtracted from further carbon balance accounting.

[92] The mobilization of stored carbohydrate reserves is modeled simplistically. There is plentiful evidence that carbohydrate reserves are formed late in a growing season, partially depleted during winter through maintenance respiration, and that a massive mobilization of reserves occurs during spring to enhance leaf onset and permit plant to photosynthesize more efficiently [*Chapin et al.*, 1990; *Dickinson et al.*, 2002; *Pregitzer*, 2003; *Krinner et al.*, 2005; *Gough et al.*, 2009]. For this reason, carbohydrate translocation is modeled to occur only during the phenological state of maximum growth (see Section 6.5) with a prescribed constant rate, $T_{rC} [gC\,m^{-2}\,PFT\,day^{-1}]$, which is *PFT*-dependent. A complete description of the allocation and translocation schemes can be found in the auxiliary material.

6.3. Tissue Turnover and Leaf Environmental Stresses

[93] A parameterization of transformation of leaves and fine roots into litter, and the conversion of living sapwood to dead sapwood/heartwood is necessary to account for the process of organic matter turnover [*Sitch et al.*, 2003; *Arora and Boer*, 2005; *Sato et al.*, 2007; *Ivanov et al.*, 2008]. The amount of sapwood biomass converted to heartwood, $S_{sapw} [gC\,m^{-2}\,PFT\,day^{-1}]$, and the turnover of fine root biomass to litter, $S_{root} [gC\,m^{-2}\,PFT\,day^{-1}]$, are linear functions of biomass and are parameterized based on tissue longevity [*Foley et al.*, 1996; *Gill and Jackson*, 2000; *Kucharik et al.*, 2000; *Bonan et al.*, 2003; *Arora and Boer*, 2005; *Wramneby et al.*, 2008]. The turnover rate of green aboveground biomass, $S_{leaf} [gC\,m^{-2}\,PFT\,day^{-1}]$, is a linear function of leaf biomass. It further depends on three turnover rates: these are related to phenology and leaf age [*Krinner et al.*, 2005; *Fatichi*, 2010], as well as to environmental stresses, such as drought and cold stresses [*Cox*, 2001; *Kozlowski and Pallardy*, 2002; *Levis et al.*, 2004; *Arora and Boer*, 2005; *Ivanov et al.*, 2008; *Fatichi*, 2010].

6.4. Carbon Balance

[94] The mass balance of carbon pools is simulated using a system of ordinary differential equations [*Dickinson et al.*, 1998; *Cayrol et al.*, 2000; *Nouvellon et al.*, 2000; *Arora and Boer*, 2005; *Ivanov et al.*, 2008]. When the net primary production is positive, the carbon change in the pools is obtained as follows:

$$\frac{dC_{leaf}}{dt} = f_l NPP - S_{leaf} + Tr_l, \tag{17}$$

$$\frac{dC_{sapw}}{dt} = f_s NPP - S_{sapw}, \tag{18}$$

$$\frac{dC_{root}}{dt} = f_r NPP - S_{root} + Tr_r, \tag{19}$$

$$\frac{dC_{hydr}}{dt} = f_h NPP - Tr_C, \tag{20}$$

where T_{rC} is subdivided into translocations to green aboveground biomass, $Tr_l [gC\,m^{-2}\,PFT\,day^{-1}]$, and fine roots, $Tr_r [gC\,m^{-2}\,PFT\,day^{-1}]$.

[95] When *NPP* is negative, the gross primary production, less growth respiration rate, is partitioned among the pools. The respective maintenance respiration costs are then subtracted from the carbon pools.

6.5. Vegetation Phenology

[96] Leaf phenology describes the seasonal cycle of canopy state. It has been recognized that phenology is mainly influenced by meteorological conditions (warm and cold periods), soil moisture, length of photoperiod, and ability to maintain positive carbon balance by plants [*Botta et al.*, 2000; *Arora and Boer*, 2005; *Ivanov et al.*, 2008].

[97] Phenology stages are modeled according to characteristics of a *PFT*. For example, evergreen, winter deciduous, drought deciduous, or raingreen vegetation types exhibit different relative sensitivities with respect to soil moisture and temperature. Four phenological states are considered in T&C [*Arora and Boer*, 2005]: dormant ($\Phi=1$), maximum growth ($\Phi=2$), normal growth ($\Phi=3$), and senescence ($\Phi=4$). The phenology states determine plant allocation patterns. The parameterizations of transitions among the four different states are formulated as functions of environmental conditions and detailed in the auxiliary material.

[98] Leaf age is parameterized similar to *Krinner et al.* [2005] in order to account for different effects of age on leaf shedding, as described in Section 6.3. An average value of green biomass age for each *PFT* is computed in T&C.

7. Model Confirmation

[99] Several case studies have been used to test the capability of Tethys-Chloris to reproduce energy fluxes, vegetation productivity metrics, and soil moisture and snowpack dynamics. Only two applications are presented in the following. The two case studies are characterized by different climates and vegetation types and

include a desert shrub community in Arizona, U.S.A. (Lucky Hills), and sagebrush plants in a snow-dominated environment in Idaho, U.S.A. (Reynolds Creek Mountain East). The two case studies are extended to simulation experiments at the watershed scale in the companion paper [*Fatichi et al.*, 2012]. All of the locations and the corresponding datasets have been described in previously published research. Only brief descriptions are provided in the following.

[100]   In the presented simulation experiments, a flat, plot-scale domain is assumed, i.e., no lateral effects such as surface/subsurface inflows or local and remote obstructions of shortwave radiation are considered. The initial conditions for soil moisture and vegetation carbon pool are obtained after spinning up the model with a simulation of the same duration as the analyzed period. A single vegetation layer, *low-vegetation*, such as shrubs (for Lucky Hills site) and sagebrush (for Reynolds Creek site) is used in the analyzed cases. A free drainage condition is assumed at the bottom of the soil column. Given the uncertainty in estimating the corresponding parameters in absence of in situ data, the soil sealing formation is enabled only for the Lucky Hills location that has a soil type similar to the one parameterized by *Mualem et al.* [1990]. Furthermore, the Lucky Hills site with a sparse vegetation cover corresponds to a location where soil

sealing is expected to produce the most significant effect.

7.1.   Lucky Hills, Arizona, USA

[101]   The Lucky Hills experimental site (110.30W, 31.44N; elevation 1372 [m $a.s.l.$]) is located within the Walnut Gulch Experimental Watershed, near Tombstone in the south-eastern Arizona. A flux tower was deployed in 1996 to measure mass and energy exchanges [*Emmerich and Verdugo*, 2008]. The flux tower footprint is composed of a sparse shrub community, mainly represented by evergreen shrubs, such as creosotebush (*Larrea tridentata*) and tarbush (*Flourensia cernua*), and deciduous shrubs, such as whitethorn acacia (*Acacia constricta*) [*King et al.*, 2008; *Skirvin et al.*, 2008]. The climate at the site can be classified as semiarid, almost arid desert-type. The mean annual temperature is 17.2 [$°C$] and the mean annual precipitation is ~333 [mm] [*Keefer et al.*, 2008]. A more detailed description of the site characteristics can be found in *Fatichi et al.* [2012, and references therein].

[102]   The model simulation spans a 13.5-year period (July 1996 through December 2009) and considers a plot-scale representation of surface composed of whitethorn acacia (C_{crown}=0.25) and creosotebush (C_{crown}= 0.10). A 2-m soil column depth is assumed for simulations. Soil hydraulic properties are derived from pedotransfer
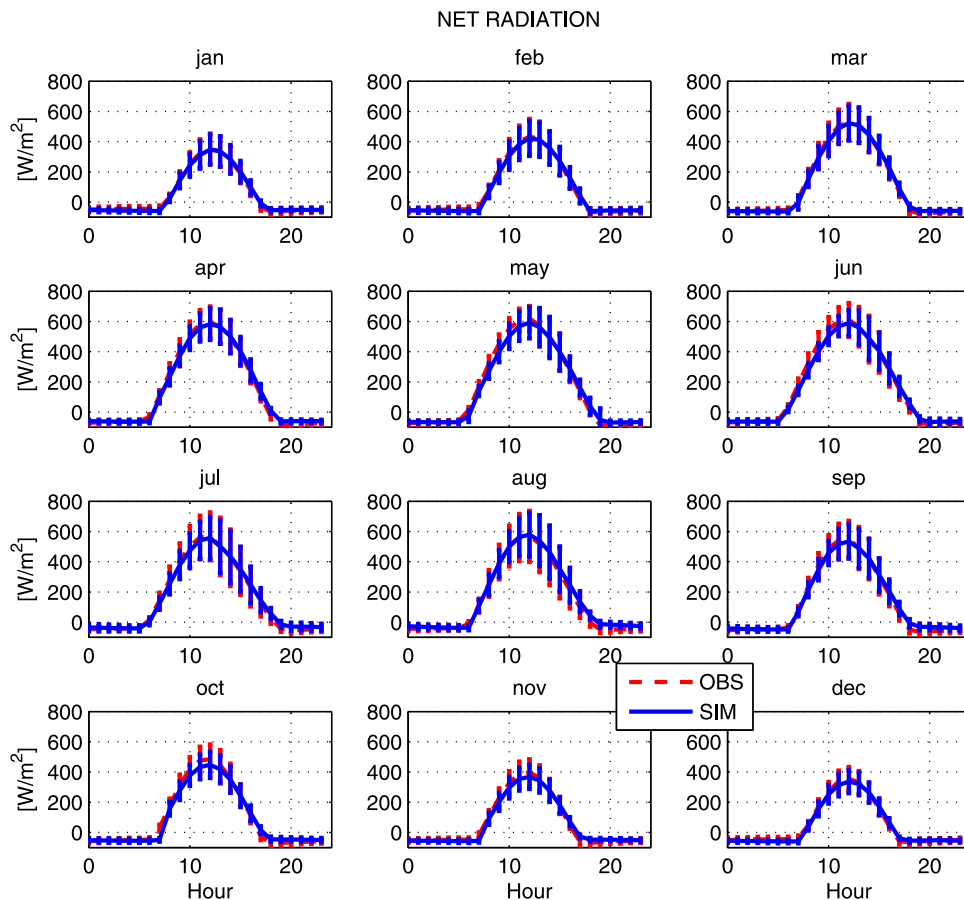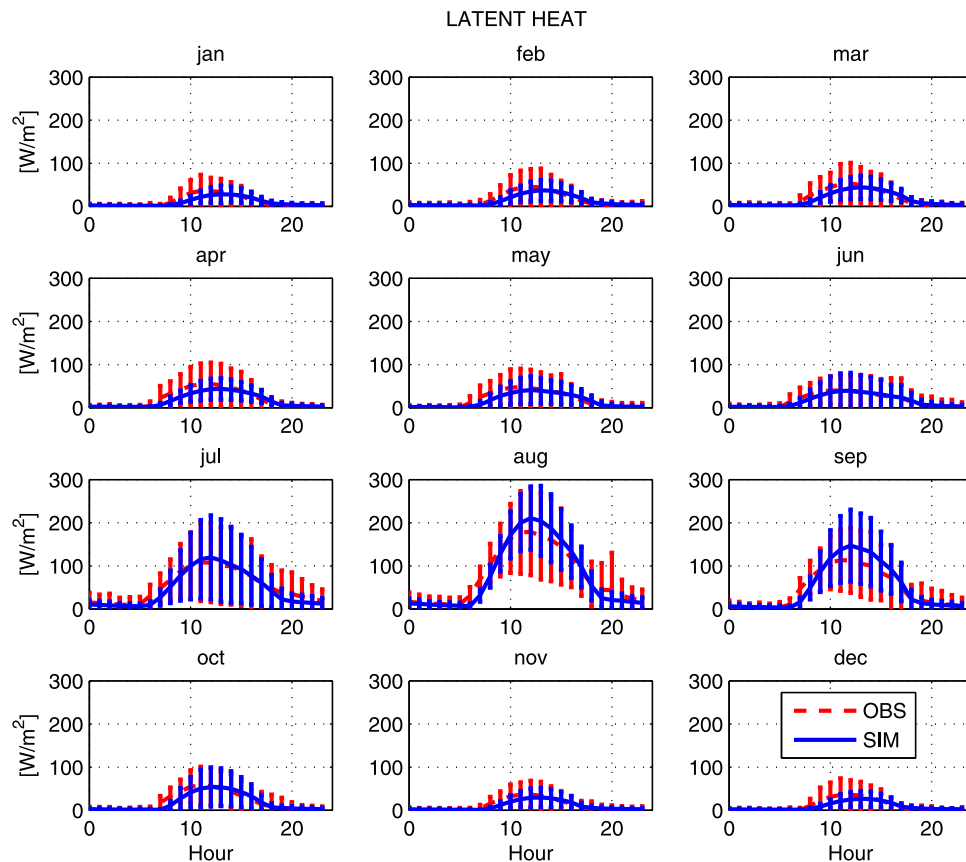

Figure 5.   A comparison between the observed (OBS) and simulated (SIM) monthly average daily cycles of net radiation, R_n. The vertical bars represent the standard deviations. The location is the Lucky Hills flux tower.

functions using 0.75 fraction of sand, 0.10 fraction of clay, and 0.01 of soil organic material [*Saxton and Rawls*, 2006]. The hydraulic conductivity is assumed to decline exponentially with depth according to the values provided by *Scott et al.* [2000]. The exact parameters used in the simulations are described in Table 1 of Text S1 in the auxiliary material.

[103] The capability of the model to reproduce the daily cycles of the mean and the standard deviation of net radiation, sensible heat, latent heat, and ground heat is illustrated in Figures 5–7. As seen, the simulation results are highly satisfactory. The results are consistent for each month: a nearly perfect match between the observed and simulated values can be inferred in the figures. A slight overestimation of latent heat fluxes is characteristic for July and August (Figure 6) as well as a general lag of the simulated sensible and latent heat fluxes early in the morning can be observed. The standard deviations of the observed and simulated fluxes at the hourly scale are almost identical for R_n and H. The observed λE exhibits a higher variability during the winter months, as compared to simulations. The determination coefficients, R^2, over the entire simulation period are $R^2=0.97$ for R_n, $R^2=0.90$ for H, $R^2=0.64$ for λE, and $R^2=0.77$ for G. It should be noted that such a performance is obtained for a period of simulation longer than 13 years and that statistics are computed at the hourly scale.

[104] The performance of the model in reproducing soil moisture dynamics is illustrated in Figure 8 at four characteristic depths. At the depths of 5 [*cm*] and 15 [*cm*], two different observed time series are shown because sensors were installed at different locations and functioned during different periods. There is a certain difference between the observed values that underlines the uncertainties present in point soil moisture measurements. The match between the simulated and observed soil moisture series in the shallower layers, i.e., at 5 [*cm*] and 15 [*cm*] depths, is satisfactory, although occasional differences can be observed (Figure 8). In deeper layers, at 30 [*cm*] and 50 [*cm*] depths, the model has a consistent performance and the simulated and observed series are very close. The lack of soil moisture measurements over the first six years, during which three significant moisture pulses reached deeper soil layers, prevents the possibility of corroborating the modeling results. However, given the fact that hydraulic properties of soil were estimated from pedotransfer functions and not in situ data, the model performance can be considered as highly satisfactory.

[105] A comparison of simulations and observations in terms of vegetation productivity and leaf area index is carried out using remote sensing data from the Moderate Resolution Imaging Spectroradiometer (MODIS). Although the latter contains numerous uncertainties and aggregates surface characteristics over a different

Figure 6. A comparison between the observed (OBS) and simulated (SIM) monthly average daily cycles of latent heat, λE. The vertical bars represent the standard deviations. The location is the Lucky Hills flux tower.
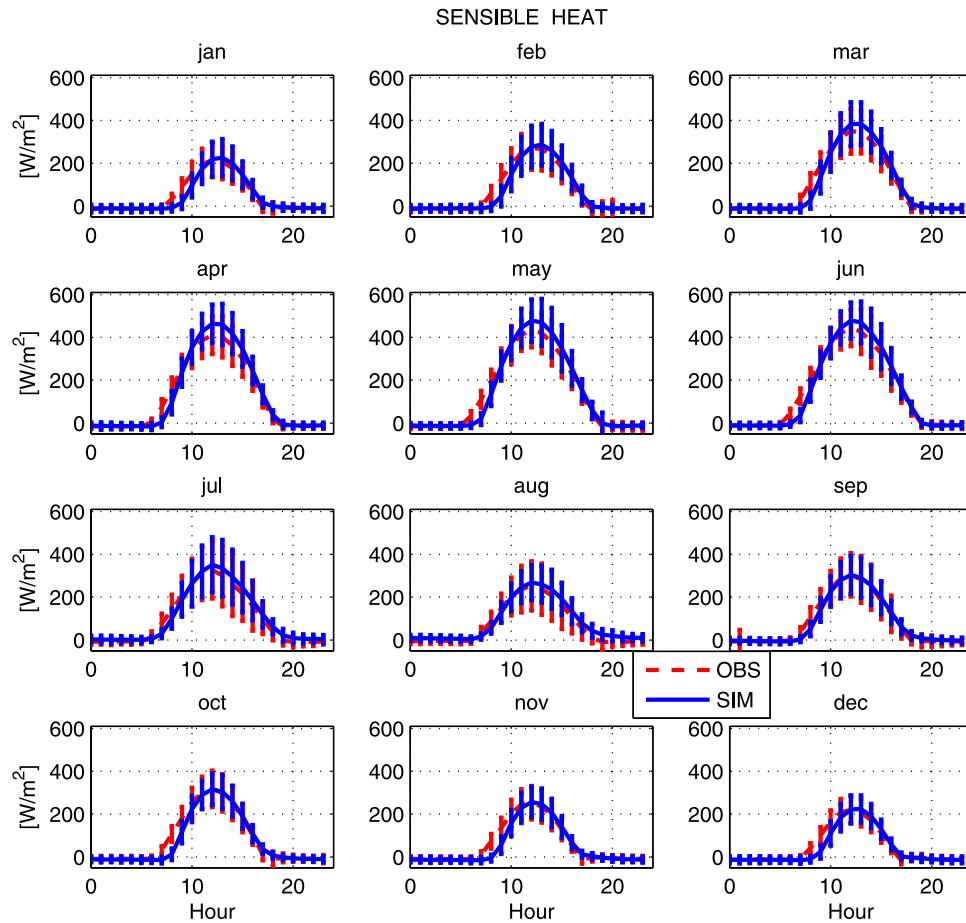
SENSIBLE HEAT

Figure 7. A comparison between the observed (OBS) and simulated (SIM) monthly average daily cycles of sensible heat, H. The vertical bars represent the standard deviations. The location is the Lucky Hills flux tower.

spatial scale, MODIS data provide a qualitatively consistent indication of canopy dynamics for the area of interest. The calculated average annual Gross Primary Production is 208 [$gC\ m^{-2}\ ground\ yr^{-1}$], the Net Primary Production is 108 [$gC\ m^{-2}\ ground\ yr^{-1}$], and the Aboveground Net Primary Production is 79 [$gC\ m^{-2}\ ground\ yr^{-1}$]. As can be observed in Figure 9a, the simulated values of GPP are generally higher than those estimated from remote sensing data, except during the period of 2006–2008, when they are comparable. Note that during the same period, LAI inferred from remote sensing observations is larger than the simulated LAI (Figure 9b). Such an overestimation can be related to the static vegetation fraction, C_{veg}=0.35, assumed for the entire simulation and/or to a mismatch between the footprint of MODIS observations (1 km^2) and the simulated area (plot-scale). There is also a pronounced inter-annual variability of vegetation productivity, as expected for a semiarid system, mainly caused by monsoon precipitation. A late monsoon season in 2004 and a drought period in 2006 can be appreciated in GPP of both simulated and remote sensing time series.

[106] The leaf area index dynamics are captured sufficiently well, as far as the magnitudes and the interannual cycle are concerned (Figure 9b). The major difference in

the LAI peaks can be observed in the years of 2007 and 2008 during which the modeled biomass still "recovers" from the 2006 drought. Such a possible long-term effect appears to be much less evident in the satellite data. Nonetheless, the capability to capture the phenological cycle of vegetation and the length of the growing season is largely confirmed.

[107] The overall performance of the model in terms of vegetation dynamics is considered to be highly satisfactory, despite a certain mismatch with the MODIS observations. It should be noted that a corroboration of simulated *LAI* and vegetation productivity with inferences from remote sensing observations is always quite uncertain. The differences in the footprint size and the indirect, approximate nature of inferences from satellite observations can indeed undermine the reliability of a comparison.

7.2. Reynolds Creek Mountain East, Idaho, USA

[108] The Reynolds Creek Mountain East watershed is located in the Owyhee Mountains, 80 km southwest of Boise, Idaho [*Slaughter et al.*, 2001]. Hourly meteorological variables, snow water equivalent, snow depth and soil moisture were collected at two stations over a 25-year period. The first station is located at a sheltered site within a clearing of an aspen/fir grove, and the other
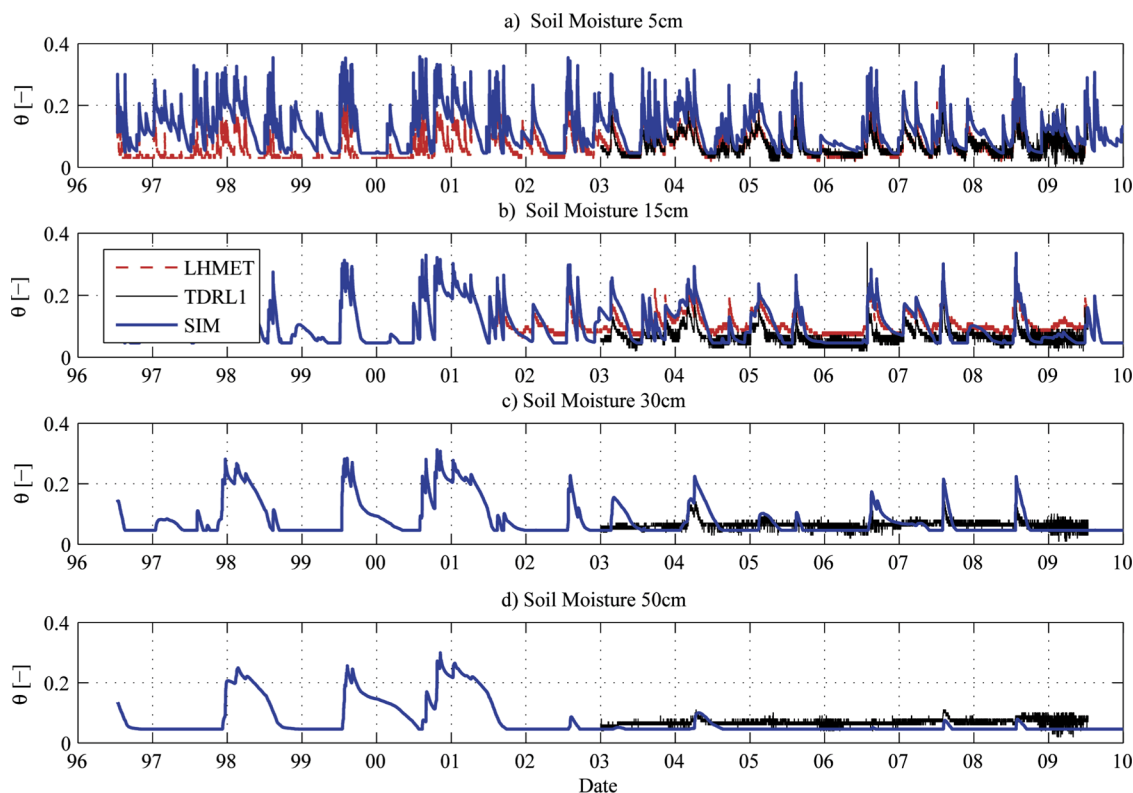
Figure 8. A comparison between the observed and simulated (SIM) soil water contents at different depths: (a) 5 cm, (b) 15 cm, (c) 30 cm, and (d) 50 cm, measured in the vicinity of the Lucky Hills flux tower. The LHMET and TDR1 represent two different time series of soil moisture measurements corresponding to the two locations close to the flux tower site.

one is located at an exposed site dominated by mixed sagebrush near the western catchment divide [*Marks et al.*, 2000; *Hanson*, 2001; *Marks et al.*, 2001; *Winstral and Marks*, 2002; *Marks et al.*, 2002; *Flerchinger et al.*, 2010; *Reba et al.*, 2011]. A more detailed description of this case study including climate and vegetation description can be found in *Fatichi et al.* [2012, and references therein]. The model simulation extends over the entire 25-year period (October 1983 through October 2008) and considers two flat sites predominantly occupied by low sagebrush (*Artemisia arbuscula*) with C_{crown}=0.90. The depth of the soil column is assigned to be 1 m [*Seyfried et al.*, 2001, 2009]. Homogeneous soil hydraulic properties are derived from pedotransfer functions for the sheltered (exposed) location using 0.376 (0.543) fraction of sand, 0.245 (0.148) fraction of clay, and 0.040 (0.025) of soil organic material. The exact parameters used in the simulations are described in Table 1 of Text S1 in the auxiliary material.

[109] The results of a simulation for the sheltered site within the Reynolds Creek Mountain East watershed are presented in the following. As Figure 10 shows, the results can be considered quite satisfactory for both the snow water equivalent and snow density. For several years, there are differences between the simulated and observed timings of the end of melting season (not clearly discerned in the figures). However, they are generally less than 150 hours. Note that no significant calibration was involved and static parameters were assumed for the entire 25 year period. The skill of the model is further testified by the high determination coefficients obtained at the hourly scale: R^2=0.95 for the snow water equivalent, S_{WE}, and R^2=0.90 for the snow depth, S_{dep}, at the bi-weekly time scale. The mean absolute error of S_{WE} simulation during the snow season is 55 [*mm*] (18% of the observed mean), computed at the hourly scale. The mean absolute error of S_{dep} is 22 [*cm*] (25% of the observed mean).

[110] The results of snow dynamics at the exposed site can only be tested against snow depth measurements over the period of 1999–2008 (not shown) because of availability reasons. Similarly, the results are satisfactory: R^2=0.89 is obtained for snow depth at the hourly scale, with the mean absolute error of 27 [*cm*] (31% of the observed mean).

[111] The sublimation/evaporation from the snowpack is estimated to be in the order of 8.0 [*mm yr^{-1}*] at the sheltered site and 54.4 [*mm yr^{-1}*] at the exposed site. These estimates can be regarded as plausible, as compared to other studies [*Gelfan et al.*, 2004; *Strasser et al.*, 2008]. The large difference in terms of snow sublimation/evaporation is due to the wind exposure characteristics of the two locations [*Winstral and Marks*, 2002].

[112] The simulated dynamics of snowpack can be considered as highly satisfactory, given the relative
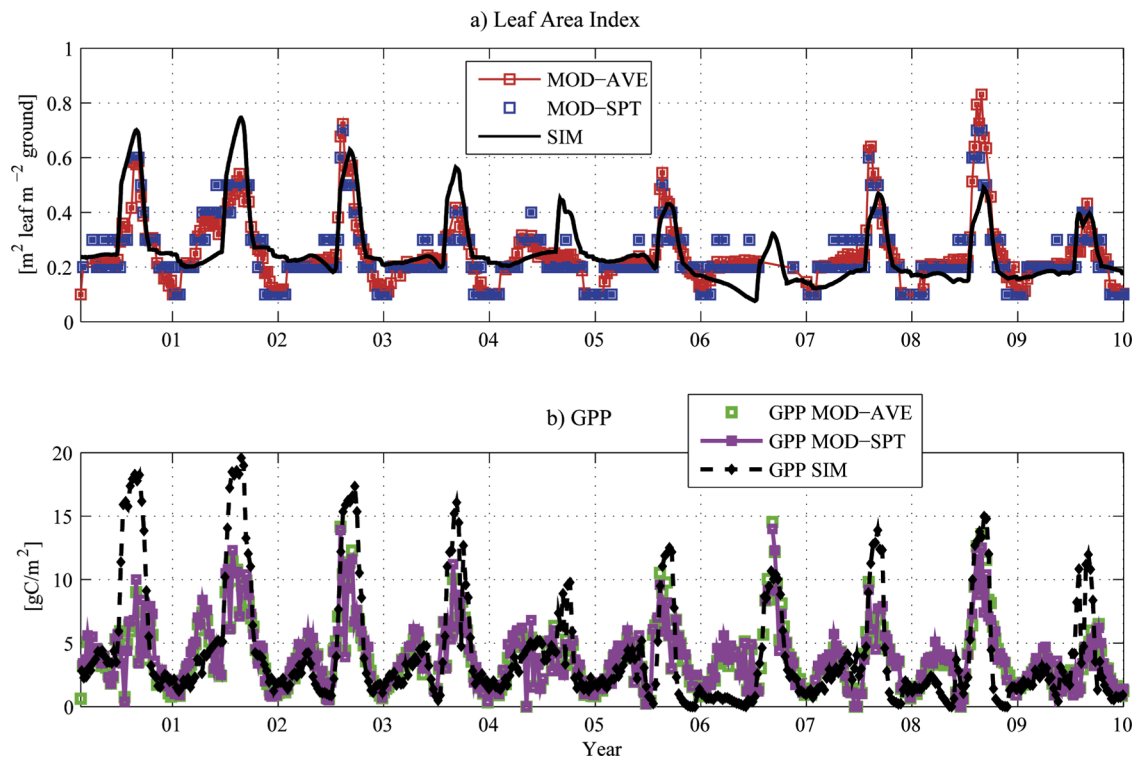
Figure 9. A comparison between the simulated (SIM) and remote sensing observation for the Lucky Hills flux tower of: (a) Leaf Area Index, (b) Gross Primary Production, GPP. "MOD-SPT" are the MODIS estimation of LAI and GPP in the pixel coinciding with the flux tower (1×1 [km^2]), "MOD-AVE" are the averages in a surrounding area of 7×7 [km^2].

simplicity of the snow-hydrology component of T&C, e.g., the representation of a single snow layer. Since both sites are open spaces covered by sagebrush, the data do not allow testing the simulation of dynamics of snow-pack below taller vegetation plants, such as aspen or fir.

[113] The model capability in reproducing soil moisture dynamics is illustrated in Figure 11, where soil water contents of the top 30 *cm* layer are compared for the sheltered and exposed sites. The model captures the timing, amplitude, and dissipation rates of soil moisture pulses quite well. Somewhat higher soil moisture peaks are characteristic of the simulated values because of the bi-weekly sampling of the observed time series (i.e., the highest values are not necessarily well represented in these series). For both sites the simulated water content tends to be closer to observations in the last 8–9 years. The determination coefficients at the bi-weekly scale for soil moisture are $R^2=0.63$ for the sheltered site and $R^2=0.73$ for the exposed site. Given the large uncertainties in the hydraulic properties of the soil (which were estimated from pedotransfer functions) and ambiguity related to the exact position of soil moisture sensors with respect to vegetation, the results are remarkably consistent.

8. Summary

[114] The current generation of catchment-scale, mechanistic ecohydrological models reflects early evolution phases of the field. Existing models exhibit varying structures with different levels of process representation

and mechanisms of coupling between hydrological and vegetation processes. This study integrates knowledge from multiple disciplines and contributes to the field a comprehensive synthesis and novel developments adapted in the form of a mechanistic ecohydrological model Tethys-Chloris. The underlying motivation is dictated by the necessity to accurately capture essential ecohydrological processes at local spatial scales and fine temporal resolutions as well as by the need to have a framework seamlessly scaleable to larger, watershed-size scales. The overarching goal of the model is to create capabilities for enhancing our understanding of the coupled vegetation-hydrology dynamics. The model theoretical basis, coupling mechanisms, and numerical solutions are regarded as a contribution to the field, facilitating the continuing progress of mechanistic models of ecohydrological processes. Furthermore, the developed model is the only mechanistic, catchment-scale ecohydrological model that can operate both in cold (with seasonal snow cover) and warm water-controlled ecosystems.

[115] The presented approach is regarded as an emerging alternative to conceptual or data-driven models that have been traditionally used to address environmental problems in a computationally efficient way with less demanding data or parameterization requirements [e.g., *Hsu et al.*, 1995; *Istanbulluoglu et al.*, 2011; *Thompson et al.*, 2011a, 2011b]. While there can be a clear benefit in using simple models [*Levin*, 1999], there are many examples where complexity cannot be fully
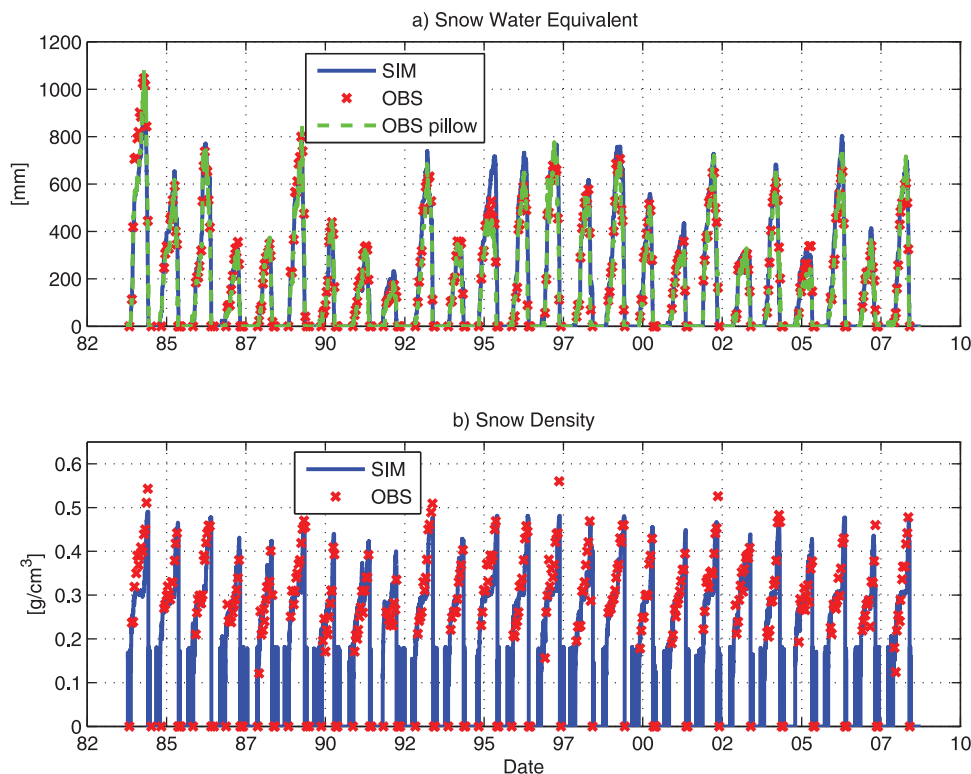
Figure 10. A comparison between the simulated and observed (a) snow water equivalent and (b) snow density at the sheltered site within the Reynolds Creek, Mountain East watershed. The solid lines are simulations (SIM), the dashed lines continuous snow-pillow observations (OBS-pillow), and the crosses represent manual observations (OBS).
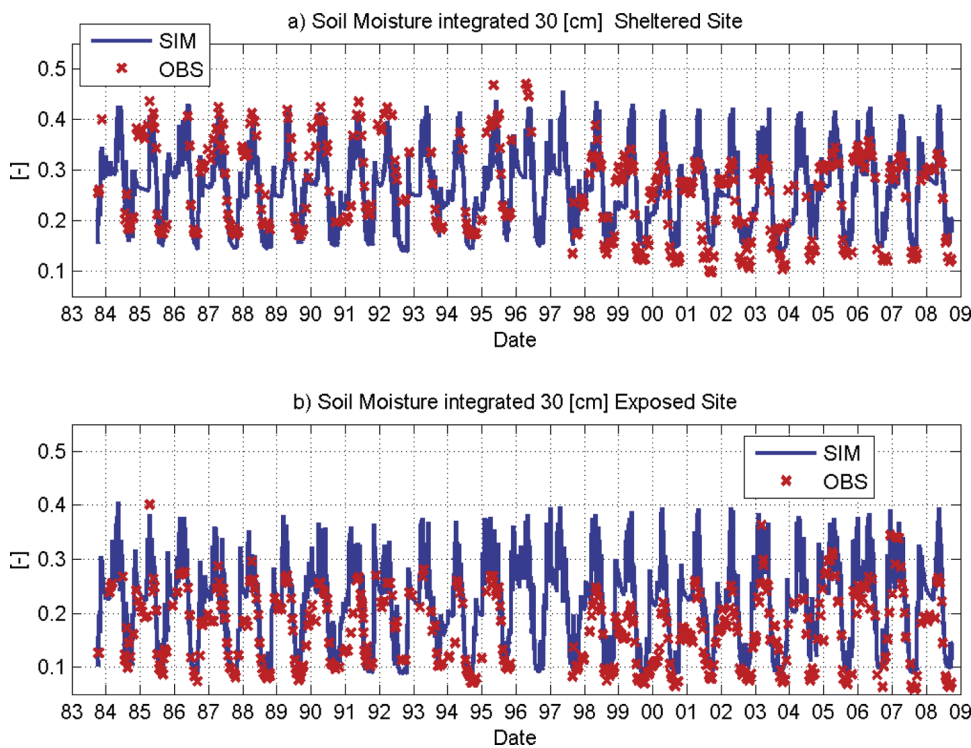
Figure 11. A comparison between the simulated (SIM) (solid line) and observed (OBS) (crosses) soil moisture integrated over the top 30 *cm* of soil (a) at the sheltered site and (b) exposed site within the Reynolds Creek, Mountain East watershed.

avoided. This is particularly the case when the aim is not only to reproduce or predict the time series of a specific variable but rather to elucidate the possible dominant driving processes and mechanisms. In other cases, there is a need to account for multiple feedbacks, such as those associated with fully transient scenarios, and the goal is to generate statement of certainty/confidence regarding the simulation results; for instance, this is the case of ecohydrological predictions of climate change effects [*Drewry et al.*, 2010b]. Furthermore, complex models are necessary when applications require transferability of solutions across scales, capability to account for specific local effects, or the simulation of non-conventional variables. In such cases process-oriented model formulations appear to be the only valid type of approach. The T&C model was designed with the objective of developing a framework for detailed/investigative studies, and providing a numerical support for testing hypotheses that concern processes and functions of natural ecohydrological systems. Through a synthesis of a wide array of process representations, the model ensures that climate, soil, vegetation, and topography collectively identify essential modes controlling ecohydrological systems, i.e., that satisfactory performance is indeed a result of appropriate mimicking of internal processes. The model can therefore be useful for designing and simulating virtual experiments as well as for providing quantitative analysis of processes that are difficult to observe in the field or reproduce with simpler models.

[116] The structure and the process components of Tethys-Chloris have been succinctly discussed (a more detailed description is provided in the auxiliary material). The paper builds on the presentation of one-dimensional formulation at the scale of a basic computational element with a subsequent integration to the level of spatial variability of a landscape. Specifically, the model solves governing equations at the local spatial scales and fine temporal resolutions, capturing the essential biotic and abiotic effects on the exchanges of energy, water, and carbon dioxide between the land-surface and the atmospheric surface layer. Embedded vegetation and hydrological models are fully coupled, e.g., processes such as photosynthesis and temporal evolution of canopy are controlled by water availability that, in turn, is controlled by plant transpiration. Spatial, quasi-three-dimensional interactions in the watershed system are introduced by routing water mass through surface and subsurface layers following topographic gradients.

[117] Tethys-Chloris was explicitly designed to have the capability of representing several vegetation species. Non-conventional horizontal and vertical compositions of plant functional types within the same computational element were made numerically feasible. The inclusion of snowpack dynamics and snow canopy interception allows the simulation of ecohydrological processes in both warm and cold environments. This permits, for example, an investigation of complex topography-snow-vegetation interactions in mountainous watersheds.

[118] The results of two case studies are presented in this work, with the overall purpose of confirming the model simulation skill over the long-term for systems with different predominant processes. The case study of Lucky Hills basin was used to address the model capability of reproducing the energy partition and vegetation seasonality and response to soil moisture. The model demonstrates a satisfactory performance for this semi-arid, warm climate. While certain differences between the simulated and observed metrics, such as latent and sensible heat, soil moisture, and vegetation productivity are acknowledged, the model demonstrates a robust skill over different temporal scales ranging from sub-daily to multi-year (13 years) periods. The case study of Reynolds Creek Mountain East was illustrative of the model skill in reproducing snowpack accumulation and melt and the consequences of these dynamics on soil water content. The performances in simulating snow depth, and soil moisture at Reynolds Creek Mountain East are robust since the characteristics of snowpack (i.e., the height, density, and snow water equivalent) are simulated consistently for a period of 25 years.

[119] Given the wide range of temporal scales and differences of represented environmental and ecosystem conditions as well as inherent uncertainties associated with data constraints and the specification of boundary conditions, the results can be in fact considered as highly satisfactory. An emerging conclusion is that a mechanistic, process-oriented structure of the model determines its simulation skill. All results for the two case studies were obtained with a minimum calibration effort, which further underlines the strength of the chosen approach and contributes factual evidence supporting the process-oriented philosophy of ecohydrological modeling. While the analysis in this work has been only limited to the plot-scale applications, the model is challenged to reproduce ecohydrological dynamics in a spatially-explicit manner at the watershed scale in a companion paper of *Fatichi et al.* [2012].

References

Abbott, M. B., J. C. Bathurst, J. A. Cunge, P. E. O'Connell, and J. Rasmussen (1986a), An introduction to the european hydrologic system-systeme hydrologique europeen, SHE, 1: History and philosophy of a physically-based, distributed modeling system, *J. Hydrol.*, *87*, 45–59, doi:10.1016/0022-1694(86)90114-9.

Abbott, M. B., J. C. Bathurst, J. A. Cunge, P. E. O'Connell, and J. Rasmussen (1986b), An introduction to the european hydrologic system-systeme hydrologique europeen, SHE, 2: Structure of a

physically-based, distributed modeling system, *J. Hydrol.*, *87*, 61–77, doi:10.1016/0022-1694(86)90115-0.

Abdella, K., and N. A. McFarlane (1996), Parameterization of the surface-layer exchange coefficients for atmospheric models, *Boundary Layer Meteorol.*, *80*, 223–248.

Abdelnour, A., M. Stieglitz, F. Pan, and R. McKane (2011), Catchment hydrological responses to forest harvest amount and spatial pattern, *Water Resour. Res.*, *47*, W09521, doi:10.1029/2010WR010165.

Anderson, E. A. (1968), Development and testing of snow pack energy balance equations, *Water Resour. Res.*, *4*(1), 19–37, doi:10.1029/WR004i001p00019.

Arain, M. A., F. Yuan, and T. A. Black (2006), Soil-plant nitrogen cycling modulated carbon exchanges in a western temperate conifer forest in Canada, *Agric. For. Meteorol.*, *140*, 171–192, doi:10.1016/j.agrformet.2006.03.021.

Arora, V. (2002), Modeling vegetation as a dynamic component in soil-vegetation-atmosphere transfer schemes and hydrological models, *Rev. Geophys.*, *40*(2), 1006., doi:10.1029/2001RG000103.

Arora, V. K., and G. J. Boer (2005), A parameterization of leaf phenology for the terrestrial ecosystem component of climate models, *Global Change Biol.*, *11*(1), 39–59, doi:10.1111/j.1365-2486.2004.00890.x.

Arya, S. P. (2001), *Introduction to Micrometeorology*, 2nd ed., Academic, San Diego, Calif.

Assmann, S. M. (1999), The cellular basis of guard cell sensing to rising CO_2, *Plant Cell Environ.*, *22*, 629–637, doi:10.1046/j.1365-3040.1999.00408.x.

Assouline, S. (2004), Rainfall-induced soil surface sealing: A critical review of observations, conceptual models, and solutions, *Vadose Zone J.*, *3*, 570–591.

Assouline, S. and Y. Mualem (1997), Modeling the dynamics of seal formation and its effect on infiltration as related to soil and rainfall characteristics, *Water Resour. Res.*, *33*(7), 1527–1536, doi:10.1029/96WR02674.

Assouline, S. and Y. Mualem (2001), Soil seal formation and its effect on infiltration: Uniform versus nonuniform seal approximation, *Water Resour. Res.*, *37*(2), 297–305, doi:10.1029/2000WR900275.

Baldocchi, D. D., and K. B. Wilson (2001), Modeling CO_2 and water vapor exchange of a temperate broadleaved forest across hourly to decadal time scales, *Ecol. Modell.*, *142*, 155–184, doi:10.1016/S0304-3800(01)00287-3.

Ball, J. T., I. E. Woodrow, and J. A. Berry (1987), A model predicting stomatal conductance and its contribution to the control of photosynthesis under different environmental conditions, in *Progress in Photosynthesis Research*, edited by J. Biggins, pp. 221–224, Martinus Nijhoff, Dordrecht, Netherlands.

Band, L. E., P. Patterson, R. Nemani, and S. W. Running (1993), Forest ecosystem processes at the watershed scale: Incorporating hillslope hydrology, *Agric. For. Meteorol.*, *63*, 93–126, doi:10.1016/0168-1923(93)90024-C.

Bartelt, P., and M. Lehning (2002), A physical SNOWPACK model for the Swiss avalanche warning. Part I: Numerical model, *Cold Reg. Technol.*, *35*, 123–145, doi:10.1016/S0165-232X(02)00074-5.

Belair, S., R. Brown, J. Mailhot, B. Bilodeau, and L.-P. Crevier (2003), Operational implementation of the ISBA land surface scheme in the Canadian regional weather forecast model. Part II: Cold season results, *J. Hydrometeorol.*, *4*, 371–386, doi:10.1175/1525-7541(2003)4<371:OIOTIL>2.0.CO;2.

Bertoldi, G., R. Rigon, and T. M. Over (2006a), Impact of watershed geomorphic characteristics on the energy and water budgets, *J. Hydrometeorol.*, *7*, 389–403, doi:10.1175/JHM500.1.

Bertoldi, G., R. Rigon, D. Tamanini, and F. Zanotti (2006b), GEOtop version 0.875: Technical description and programs guide, *Tech. Rep. dica-06-001*, Univ. of Trento, Trento, Italy.

Beven, K. J., and J. Freer (2001), A dynamic TOPMODEL, *Hydrol. Processes*, *15*, 1993–2011, doi:10.1002/hyp.252.

Beven, K. J., and M. J. Kirkby (1979), A physically based, variable contributing area model of basin hydrology, *Hydrol. Sci. Bull.*, *24*, 43–69, doi:10.1080/02626667909491834.

Bewley, D., R. Essery, J. Pomeroy, and C. Ménard (2010), Measurements and modelling of snowmelt and turbulent heat fluxes over shrub tundra, *Hydrol. Earth Syst. Sci.*, *14*, 1331–1340, doi:10.5194/hess-14-1331-2010.

Bonan, G. B. (1996), A land surface model (LSM version 1.0) for ecological, hydrological, and atmospheric studies: Technical description and user's guide, *NCAR Tech. Note NCAR/TN-417*, Natl. Cent. for Atmos. Res., Boulder, Colo.

Bonan, G. B. (2002), *Ecological Climatology: Concept and Applications*, Cambridge Univ. Press, New York.

Bonan, G. B. (2008), Forests and climate change: Forcings, feedbacks, and the climate benefits of forests, *Science*, *320*, 1444–1449, doi:10.1126/science.1155121.

Bonan, G. B., S. Levis, L. Kergoat, and K. W. Oleson (2002), Landscapes as patches of plant functional types: An integrating concept for climate and ecosystem models, *Global Biogeochem. Cycles*, *16*(2), 1021, doi:10.1029/2000GB001360.

Bonan, G. B., S. Levis, S. Sitch, M. Vertenstein, and K. W. Oleson (2003), A dynamic global vegetation model for use with climate models: Concepts and description of simulated vegetation dynamics, *Global Change Biol.*, *9*, 1543–1566, doi:10.1046/j.1365-2486.2003.00681.x.

Bond, B. (2003), Hydrology and ecology meet-and the meeting is good, *Hydrol. Processes*, *17*, 2087–2089, doi:10.1002/hyp.5133.

Botta, A., N. Viovy, P. Ciais, and P. Friedlingstein (2000), A global prognostic scheme of leaf onset using satellite data, *Global Change Biol.*, *6*, 709–726, doi:10.1046/j.1365-2486.2000.00362.x.

Botter, G., S. Zanardo, A. Porporato, I. Rodriguez-Iturbe, and A. Rinaldo (2008), Ecohydrological model of flow duration curves and annual minima, *Water Resour. Res.*, *44*, W08418, doi:10.1029/2008WR006814.

Bras, R. L. (1990), *Hydrology: An Introduction to Hydrologic Science*, Addison-Wesley, Reading, Mass.

Brutsaert, W. (2005), *Hydrology: An Introduction*, Cambridge Univ. Press, Cambridge, U. K.

Camporese, M., C. Paniconi, M. Putti, and S. Orlandini (2010), Surface-subsurface flow modeling with path-based runoff routing, boundary condition-based coupling, and assimilation of multisource observation data, *Water Resour. Res.*, *46*, W02512, doi:10.1029/2008WR007536.

Caylor, K. K., S. Manfreda, and I. Rodriguez-Iturbe (2005), On the coupled geomorphological and ecohydrological organization of river basins, *Adv. Water Resour.*, *28*, 69–86, doi:10.1016/j.advwatres.2004.08.013.

Cayrol, P., L. Kergoat, S. Moulin, G. Dedieu, and A. Chehbouni (2000), Calibrating a coupled SVAT-vegetation growth model with remotely sensed reflectance and surface temperature—A case study for the HAPEX-Sahel grassland sites, *J. Appl. Meteorol.*, *39*(12), 2452–2472, doi:10.1175/1520-0450(2000)039<2452:CACSVG>2.0.CO;2.

Chanson, H. (2004), *The Hydraulics of Open Channel Flow: An Introduction*, Elsevier, Oxford, U. K.

Chapin, F. S., III, E.-D. Schulze, and H. A. Mooney (1990), The ecology and economics of storage in plants, *Annu. Rev. Ecol. Syst.*, *21*, 423–447, doi:10.1146/annurev.es.21.110190.002231.

Chapin, F. S., III, J. T. Randerson, A. D. McGuire, J. A. Foley, and C. B. Field (2008), Changing feedbacks in the climate-biosphere system, *Front. Ecol. Environ.*, *6*(6), 313–320, doi:10.1890/080005.

Choudhury, B. J., and J. L. Monteith (1988), A four-layer model for the heat budget of homogeneous land surfaces, *Q. J. R. Meteorol. Soc.*, *114*, 378–398, doi:10.1002/qj.49711448006.

Chow, V. T. (1988), *Applied Hydrology*, McGraw-Hill, New York.

Ciarapica, L., and E. Todini (2002), TOPKAPI: A model for the representation of the rainfall-runoff process at different scales, *Hydrol. Processes*, *16*, 207–229, doi:10.1002/hyp.342.

Collins, D. B. G. and R. L. Bras (2007), Plant rooting strategies in water-limited ecosystems, *Water Resour. Res.*, *43*, W06407, doi:10.1029/2006WR005541.

Cox, P. M. (2001), Description of the TRIFFID Dynamic Global Vegetation Model, *Tech. Note 24*, Met Off. Hadley Cent., Exeter, U. K.

Crawford, N., and R. Linsley (1966), Digital simulation on hydrology: Stanford watershed model IV, *Tech. Rep. 39*, Stanford Univ., Palo Alto, Calif.

Dai, Y., R. E. Dickinson, and Y.-P. Wang (2004), A two-big-leaf model for canopy temperature, photosynthesis, and stomatal conductance, *J. Clim.*, *17*, 2281–2299, doi:10.1175/1520-0442(2004)017<2281:ATMFCT>2.0.CO;2.

Daly, E., and A. Porporato (2005), A review of soil moisture dynamics: From rainfall infiltration to ecosystem response, *Environ. Eng. Sci.*, *22*(1), 9–24, doi:10.1089/ees.2005.22.9.

Daly, E., A. Porporato, and I. Rodriguez-Iturbe (2004), Coupled dynamics of photosynthesis, transpiration, and soil water balance. Part I: Upscaling from hourly to daily level, *J. Hydrometeorol.*, *5*, 546–558, doi:10.1175/1525-7541(2004)005<0546:CDOPTA>2.0.CO;2.

de Pury, D. G. G., and G. D. Farquhar (1997), Simple scaling of photosynthesis from leaves to canopies without the errors of big-leaf models, *Plant Cell Environ.*, *20*(5), 537–557, doi:10.1111/j.1365-3040.1997.00094.x.

Deardorff, J. W. (1978), Efficient prediction of ground surface temperature and moisture, with inclusion of a layer of vegetation, *J. Geophys. Res.*, *83*(C4), 1889–1903, doi:10.1029/JC083iC04p01889.

Deckmym, G., H. Verbeeck, M. O. de Beeck, D. Vansteenkiste, K. Steppe, and R. Ceulemans (2008), ANAFORE: A stand-scale process-based forest model that includes wood tissue development and labile carbon storage in trees, *Ecol. Modell.*, *215*, 345–368, doi:10.1016/j.ecolmodel.2008.04.007.

Dewar, R. C. (2002), The Ball-Berry-Leuning and Tardieu-Davies stomatal models: Synthesis and extension within a spatially aggregated picture of guard cell function, *Plant Cell Environ.*, *25*, 1383–1398, doi:10.1046/j.1365-3040.2002.00909.x.

Dickinson, R. E. (1983), Land surface processes and climate-surface albedos and energy balance, *Adv. Geophys.*, *25*, 305–353, doi:10.1016/S0065-2687(08)60176-4.

Dickinson, R. E., A. Henderson-Sellers, and P. J. Kennedy (1993), Biosphere-atmosphere transfer scheme (BATS) version 1E as coupled to the NCAR Community Climate Model, *NCAR Tech. Note NCAR/TN-387+STR*, Natl. Cent. for Atmos. Res., Boulder, Colo.

Dickinson, R. E., M. Shaikh, R. Bryant, and L. Graumlich (1998), Interactive canopies for a climate model, *J. Clim.*, *11*, 2823–2836, doi:10.1175/1520-0442(1998)011<2823:ICFACM>2.0.CO;2.

Dickinson, R. E., et al. (2002), Nitrogen controls on climate model evapotranspiration, *J. Clim.*, *15*, 278–294, doi:10.1175/1520-0442(2002)015<0278:NCOCME>2.0.CO;2.

Dingman, S. L. (1994), *Physical Hydrology*, Prentice-Hall, Upple Saddle River, N. J.

Douville, H., J.-F. Royer, and J.-F. Mahfouf (1995), A new snow parameterization for the Meteo-France climate model. Part I: Validation in stand-alone experiments, *Clim. Dyn.*, *12*, 21–35, doi:10.1007/BF00208760.

Drewry, D. T., P. Kumar, S. Long, C. Bernacchi, X.-Z. Liang, and M. Sivapalan (2010a), Ecohydrological responses of dense canopies to environmental variability: 1. Interplay between vertical structure and photosynthetic pathway, *J. Geophys. Res.*, *115*, G04022, doi:10.1029/2010JG001340.

Drewry, D. T., P. Kumar, S. Long, C. Bernacchi, X.-Z. Liang, and M. Sivapalan (2010b), Ecohydrological responses of dense canopies to environmental variability: 2. Role of acclimation under elevated CO_2, *J. Geophys. Res.*, *115*, G04023, doi:10.1029/2010JG001341.

Dubayah, R., and S. Loechel (1997), Modeling topographic solar radiation using GOES data, *J. Appl. Meteorol.*, *36*, 141–154, doi:10.1175/1520-0450(1997)036<0141:MTSRUG>2.0.CO;2.

Eagleson, P. S. (2002), *Ecohydrology: Darwinian Expression of Vegetation Form and Function*, Cambridge Univ. Press, Cambridge, U. K.

Ebel, B. A., K. Loague, D. R. Montgomery, and W. E. Dietrich (2008), Physics-based continuous simulation of long-term near-surface hydrologic response for the Coos Bay experimental catchment, *Water Resour. Res.*, *44*, W07417, doi:10.1029/2007WR006442.

Ellis, C. R., J. W. Pomeroy, T. Brown, and J. MacDonald (2010), Simulation of snow accumulation and melt in needleleaf forest environments, *Hydrol. Earth Syst. Sci.*, *14*, 925–940, doi:10.5194/hess-14-925-2010.

Emanuel, R. E., H. E. Epstein, B. L. McGlynn, D. L. Welsch, D. J. Muth, and P. D'Odorico (2010), Spatial and temporal controls on watershed ecohydrology in the northern Rocky Mountains, *Water Resour. Res.*, *46*, W11553, doi:10.1029/2009WR008890.

Emmerich, W. E. and C. L. Verdugo (2008), Long-term carbon dioxide and water flux database, Walnut Gulch Experimental Watershed, Arizona, United States, *Water Resour. Res.*, *44*, W05S09, doi:10.1029/2006WR005693.

Essery, R., E. Martin, H. Douville, A. Fernandez, and E. Brun (1999), A comparison of four snow models using observations from an alpine site, *Clim. Dyn.*, *15*, 583–593, doi:10.1007/s003820050302.

Essery, R., N. Rutter, J. Pomeroy, R. Baxter, M. Stähli, D. Gustafsson, A. Barr, P. Bartlett, and K. Elder (2009), SNOWMIP2: An evaluation of forest snow process simulations, *Bull. Am. Meteorol. Soc.*, *90*(8), 1120–1135, doi:10.1175/2009BAMS2629.1.

Farquhar, G. D. (1989), Models of integrated photosynthesis of cells and leaves, *Philos. Trans. R. Soc. B*, *323*, 357–367, doi:10.1098/rstb.1989.0016.

Fatichi, S. (2010), The modeling of hydrological cycle and its interaction with vegetation in the framework of climate change, PhD thesis, Univ. of Florence, Florence, Italy.

Fatichi, S., V. Y. Ivanov, and E. Caporali (2011), Simulation of future climate scenarios with a weather generator, *Adv. Water Resour.*, *34*, 448–467, doi:10.1016/j.advwatres.2010.12.013.

Fatichi, S., V. Y. Ivanov, and E. Caporali (2012), A mechanistic ecohydrological model to investigate complex interactions in cold and warm water-controlled environments: 2. Spatiotemporal analyses, *J. Adv. Model. Earth Syst.*, doi:10.1029/2011MS000087, in press.

Feddes, R. A., et al. (2001), Modeling root water uptake in hydrological and climate models, *Bull. Am. Meteorol. Soc.*, *82*(12), 2797–2809, doi:10.1175/1520-0477(2001)082<2797:MRWUIH>2.3.CO;2.

Fernandez-Illescas, C. P., A. Porporato, F. Laio, and I. Rodriguez-Iturbe (2001), The ecohydrological role of soil texture in a water-limited ecosystem, *Water Resour. Res.*, *37*(12), 2863–2872, doi:10.1029/2000WR000121.

Flerchinger, G. N., D. Marks, M. L. Reba, Q. Yu, and M. S. Seyfried (2010), Surface fluxes and water balance of spatially varying vegetation within a small mountainous headwater catchment, *Hydrol. Earth Syst. Sci.*, *14*, 965–978, doi:10.5194/hess-14-965-2010.

Foley, J. A., I. C. Prentice, N. Ramankutty, S. Levis, D. Pollard, S. Sitch, and A. Haxeltine (1996), An integrated biosphere model of land surface processes, terrestrial carbon balance, and vegetation dynamics, *Global Biogeochem. Cycles*, *10*(4), 603–628, doi:10.1029/96GB02692.

Freeze, R. A. (1971), Three-dimensional, transient, saturated-unsaturated flow in a groundwater basin, *Water Resour. Res.*, *7*(2), 347–366, doi:10.1029/WR007i002p00347.

Freeze, R. A. (1972), Role of subsurface flow in generating surface runoff: 1. Base flow contributions to channel flow, *Water Resour. Res.*, *8*(3), 609–623, doi:10.1029/WR008i003p00609.

Friedlingstein, P., G. Joel, C. B. Field, and I. Fung (1998), Toward an allocation scheme for global terrestrial carbon models, *Global Change Biol.*, *5*, 755–770, doi:10.1046/j.1365-2486.1999.00269.x.

Friend, A. D., A. K. Stevens, R. G. Knox, and M. G. R. Cannell (1997), A process-based, terrestrial biosphere model of ecosystem dynamics (Hybrid v3.0), *Ecol. Modell.*, *95*, 249–287, doi:10.1016/S0304-3800(96)00034-8.

Garratt, J. R. (1992), *The Atmospheric Boundary Layer*, Cambridge Univ. Press, Cambridge, U. K.

Garrote, L., and R. L. Bras (1995), A distributed model for real-time flood casting using digital elevation models, *J. Hydrol.*, *167*, 279–306, doi:10.1016/0022-1694(94)02592-Y.

Gelfan, A. N., J. W. Pomeroy, and L. S. Kuchment (2004), Modeling forest cover influences on snow accumulation, sublimation, and melt, *J. Hydrometeorol.*, *5*, 785–803, doi:10.1175/1525-7541(2004)005<0785:MFCIOS>2.0.CO;2.

Gerrits, A. M. J., H. H. G. Savenije, L. Hoffmann, and L. Pfister (2007), New technique to measure forest floor interception—An application in a beech forest in Luxembourg, *Hydrol. Earth Syst. Sci.*, *11*, 695–701, doi:10.5194/hess-11-695-2007.

Gill, R. A., and R. B. Jackson (2000), Global patterns of root turnover for terrestrial ecosystems, *New Phytol.*, *147*, 13–31, doi:10.1046/j.1469-8137.2000.00681.x.

Gough, C. M., C. E. Flower, C. S. Vogel, D. Dragoni, and P. S. Curtis (2009), Whole-ecosystem labile carbon production in a north temperate deciduous forest, *Agric. For. Meteorol.*, *149*, 1531–1540, doi:10.1016/j.agrformet.2009.04.006.

Guswa, A. J., M. A. Celia, and I. Rodriguez-Iturbe (2002), Models of soil moisture dynamics in ecohydrology: A comparative study, *Water Resour. Res.*, *38*(9), 1166., doi:10.1029/2001WR000826.

Hanson, C. L. (2001), Long-term precipitation database, Reynolds Creek Experimental Watershed, Idaho, United States, *Water Resour. Res.*, *37*(11), 2831–2834, doi:10.1029/2001WR000415.

Hedstrom, N. R., and J. W. Pomeroy (1998), Measurements and modelling of snow interception in the boreal forest, *Hydrol. Processes*, *12*, 1611–1625, doi:10.1002/(SICI)1099-1085(199808/09)12:10/11<1611::AID-HYP684>3.0.CO;2-4.

Hoch, G., A. Richter, and C. Körner (2003), Non-structural carbon compounds in temperate forest trees, *Plant Cell Environ.*, *26*, 1067–1081, doi:10.1046/j.0016-8025.2003.01032.x.

Howes, D. A., and A. D. Abrahams (2003), Modeling runoff and runon in a desert shrubland ecosystem, Jornada Basin, New Mexico, *Geomorphology*, *53*, 45–73, doi:10.1016/S0169-555X(02)00347-1.

Hsu, K., H. V. Gupta, and S. Sorooshian (1995), Artificial Neural Network Modeling of the rainfall-runoff process, *Water Resour. Res.*, *31*(10), 2517–2530, doi:10.1029/95WR01955.

Hu, Z. and S. Islam (1995), Prediction of ground surface temperature and soil moisture content by the force-restore method, *Water Resour. Res.*, *31*(10), 2531–2539, doi:10.1029/95WR01650.

Idso, S. B. (1981), A set of equations for full spectrum and 8- to 14-μm and 10.5- to 12.5 μm thermal radiation from cloudless skies, *Water Resour. Res.*, *17*(2), 295–304.

Istanbulluoglu, E., T. Wang, and D. A. Wedin (2011), Evaluation of ecohydrologic model parsimony at local and regional scales in a

semiarid grassland ecosystem, *Ecohydrology*, 5(1), 121–142, doi:10. 1002/eco.211.

Ivanov, V. Y. (2006), Effects of dynamic vegetation and topography on hydrological processes in semi-arid areas, PhD thesis, Dep. of Civ. and Environ. Eng., Mass. Inst. of Technol., Cambridge.

Ivanov, V. Y., E. R. Vivoni, R. L. Bras, and D. Entekhabi (2004a), Catchment hydrologic response with a fully distributed triangulated irregular network model, *Water Resour. Res.*, 40, W11102, doi:10. 1029/2004WR003218.

Ivanov, V. Y., E. R. Vivoni, R. L. Bras, and D. Entekhabi (2004b), Preserving high-resolution surface and rainfall data in operational-scale basin hydrology: A fully-distributed physically-based approach, *J. Hydrol.*, 298, 80–111, doi:10.1016/j.jhydrol.2004.03. 041.

Ivanov, V. Y., R. L. Bras, and D. C. Curtis (2007), A weather generator for hydrological, ecological, and agricultural applications, *Water Resour. Res.*, 43, W10406, doi:10.1029/2006WR005364.

Ivanov, V. Y., R. L. Bras, and E. R. Vivoni (2008), Vegetation-hydrology dynamics in complex terrain of semiarid areas: 1. A mechanistic approach to modeling dynamic feedbacks, *Water Resour. Res.*, 44, W03429, doi:10.1029/2006WR005588.

Ivanov, V. Y., S. Fatichi, G. D. Jenerette, J. F. Espeleta, P. A. Troch, and T. E. Huxman (2010), Hysteresis of soil moisture spatial heterogeneity and the ''homogenizing''effect of vegetation, *Water Resour. Res.*, 46, W09521, doi:10.1029/2009WR008611.

Jackson, R. B., J. Canadell, J. R. Ehleringer, H. A. Mooney, O. E. Sala, and E. D. Schulze (1996), A global analysis of root distributions for terrestrial biomes, *Oecologia*, 108(3), 389–411, doi:10.1007/BF00333714.

Jost, G., M. Weiler, D. R. Gluns, and Y. Alila (2007), The influence of forest and topography on snow accumulation and melt at the watershed-scale, *J. Hydrol.*, 347, 101–115, doi:10.1016/j.jhydrol.2007.09.006.

Kampf, S. K. and S. J. Burges (2007), A framework for classifying and comparing distributed hillslope and catchment hydrologic models, *Water Resour. Res.*, 43, W05423, doi:10.1029/2006WR005370.

Kamphorst, E., V. G. Jetten, J. Guerif, J. Pitkanen, B. Iversen, J. Douglas, and A. Paz (2000), Predicting depressional storage from soil surface roughness, *Soil Sci. Soc. Am. J.*, 64, 1749–1758, doi:10. 2136/sssaj2000.6451749x.

Keefer, T. O., M. S. Moran, and G. B. Paige (2008), Long-term meteorological and soil hydrology database, Walnut Gulch Experimental Watershed, Arizona, United States, *Water Resour. Res.*, 44, W05S07, doi:10.1029/2006WR005702.

King, D. M., S. M. Skirvin, C. D. Holifield Collins, M. S. Moran, S. H. Biedenbender, M. R. Kidwell, M. A. Weltz, and A. Diaz-Gutierrez (2008), Assessing vegetation change temporally and spatially in southeastern Arizona, *Water Resour. Res.*, 44, W05S15, doi:10.1029/2006WR005850.

Knorr, W. (2000), Annual and interannual CO_2 exchanges of the terrestrial biosphere: Process based simulations and uncertainties, *Global Ecol. Biogeogr.*, 9, 225–252, doi:10.1046/j.1365-2699.2000. 00159.x.

Kollet, S. J., and R. M. Maxwell (2006), Integrated surface-groundwater flow modeling: A free-surface overland flow boundary condition in a parallel groundwater flow model, *Adv. Water Resour.*, 29, 945–958, doi:10.1016/j.advwatres.2005.08.006.

Kollet, S. J. and R. M. Maxwell (2008), Capturing the influence of groundwater dynamics on land surface processes using an integrated, distributed watershed model, *Water Resour. Res.*, 44, W02402, doi:10.1029/2007WR006004.

Kollet, S. J., R. M. Maxwell, C. S. Woodward, S. Smith, J. Vanderborght, H. Vereecken, and C. Simmer (2010), Proof of concept of regional scale hydrologic simulations at hydrologic resolution utilizing massively parallel computer resources, *Water Resour. Res.*, 46, W04201, doi:10.1029/2009WR008730.

Körner, C. (2003), Carbon limitation in trees, *J. Ecol.*, 91, 4–17, doi:10. 1046/j.1365-2745.2003.00742.x.

Kozlowski, T. T., and S. G. Pallardy (1997), *Physiology of Woody Plants*, Academic, San Diego, Calif.

Kozlowski, T. T., and S. G. Pallardy (2002), Acclimation and adaptive responses of woody plants to environmental stresses, *Bot. Rev.*, 68(2), 270–334, doi:10.1663/0006-8101(2002)068[0270:AAAROW]2. 0.CO;2.

Krinner, G., N. Viovy, N. de Noblet-Ducoudré, J. Ogée, J. Polcher, P. Friedlingstein, P. Ciais, S. Sitch, and I. C. Prentice (2005), A dynamic global vegetation model for studies of the coupled atmosphere-biosphere system, *Global Biogeochem. Cycles*, 19, GB1015, doi:10.1029/2003GB002199.

Kucharik, C. J., J. A. Foley, C. Delire, V. A. Fisher, M. T. Coe, J. D. Lenters, C. Young-Molling, N. Ramankutty, J. M. Norman, and S. T. Gower (2000), Testing the performance of a dynamic global ecosystem model: Water balance, carbon balance, and vegetation structure, *Global Biogeochem. Cycles*, 14(3), 795–825, doi:10.1029/1999GB001138.

Kumar, L., A. K. Skidmore, and E. Knowles (1997), Modeling topographic variation in solar radiation in a GIS environment, *Int. J. Geogr. Inf. Sci.*, 11, 475–497, doi:10.1080/136588197242266.

Kumar, M., G. Bhatt, and C. J. Duffy (2010), An object-oriented shared data model for GIS and distributed hydrologic models, *Int. J. Geogr. Inf. Sci.*, 24(7), 1061–1079, doi:10.1080/13658810903289460.

Laio, F., A. Porporato, L. Ridolfi, and I. Rodriguez-Iturbe. (2001), Plants in water-controlled ecosystems: active role in hydrological processes and response to water stress. II. Probabilistic soil moisture dynamics, *Adv. Water Resour.*, 24, 707–723, doi:10.1016/S0309-1708(01)00005-7.

Lee, H. S., C. J. Matthews, R. D. Braddock, G. C. Sander, and F. Gandola (2004), A MATLAB method of lines template for transport equations, *Environ. Modell. Software*, 19, 603–614, doi:10.1016/j.envsoft.2003.08.017.

Lee, Y.-H., and L. Mahrt (2004), An evaluation of snowmelt and sublimation over short vegetation in land surface modelling, *Hydrol. Processes*, 18, 3543–3557, doi:10.1002/hyp.5799.

LeRoux, X., A. Lacointe, A. Escobar-Gutiérrez, and S. LeDizès (2001), Carbon-based models of individual tree growth: A critical appraisal, *Ann. For. Sci.*, 58, 459–506, doi:10.1051/forest:2001140.

Leuning, R. (1990), Modelling stomatal behaviour and photosynthesis of eucalyptus grandis, *Aust. J. Plant Physiol.*, 17, 159–175, doi:10. 1071/PP9900159.

Leuning, R. (1995), A critical appraisal of a combined stomatal-photosynthesis model for C3 plants, *Plant Cell Environ.*, 18, 357–364, doi:10.1111/j.1365-3040.1995.tb00371.x.

Levin, S. (1999), *Fragile Dominion: Complexity and the Commons*, Perseus, Reading, Mass.

Levis, S., G. B. Bonan, M. Vertenstein, and K. W. Oleson (2004), The Community Land Model's Dynamic Global Vegetation Model (CLMDGVM): Technical description and user's guide, *NCAR Tech. Note NCAR/TN-459+IA*, Natl. Cent. for Atmos. Res., Boulder, Colo.

Liston, G. E., and K. Elder (2006), A distributed snow-evolution modeling system (SnowModel), *J. Hydrometeorol.*, 7, 1259–1276, doi:10.1175/JHM548.1.

Liston, G. E., J. P. McFadden, M. Sturm, and R. A. Pielke (2002), Modelled changes in arctic tundra snow, energy and moisture fluxes due to increased shrubs, *Global Change Biol.*, 8, 17–32, doi:10.1046/j.1354-1013.2001.00416.x.

Loague, K., and J. E. VanderKwaak (2004), Physics-based hydrologic response simulation: platinum bridge, 1958 Edsel, or useful tool, *Hydrol. Processes*, 18, 2949–2956, doi:10.1002/hyp.5737.

Loague, K., C. S. Heppner, B. B. Mirus, B. A. Ebel, Q. Ran, A. E. Carr, S. H. BeVille, and J. E. VanderKwaak (2006), Physics-based hydrologic-response simulation: Foundation for hydroecology and hydrogeomorphology, *Hydrol. Processes*, 20, 1231–1237, doi:10. 1002/hyp.6179.

Louis, J.-F. (1979), A parametric model of the vertical eddy fluxes in the atmosphere, *Boundary Layer Meteorol.*, 17, 187–202, doi:10. 1007/BF00117978.

Lüdeke, M. K. B., et al. (1994), The Frankfurt biosphere model: A global process-oriented model of seasonal and long-term CO_2 exchange between terrestrial ecosystems and the atmosphere. I. Model description and illustrative results for cold deciduous and boreal forests, *Clim. Res.*, 4(2), 143–166, doi:10.3354/cr004143.

Ma, S., D. D. Baldocchi, L. Xu, and T. Hehn (2007), Inter-annual variability in carbon dioxide exchange of an oak/grass savanna and open grassland in california, *Agric. For. Meteorol.*, 147, 157–171, doi:10.1016/j.agrformet.2007.07.008.

Mackay, D. S. (2001), Evaluation of hydrologic equilibrium in a mountainous watershed: incorporating forest canopy spatial adjustment to soil biogeochemical processes, *Adv. Water Resour.*, 24, 1211–1227, doi:10.1016/S0309-1708(01)00040-9.

Mackay, D. S., and L. E. Band (1997), Forest ecosystem processes at the watershed scale: Dynamic coupling of distributed hydrology and canopy growth, *Hydrol. Processes*, 11, 1197–1217, doi:10.1002/(SICI)1099-1085(199707)11:9<1197::AID-HYP552>3.0.CO;2-W.

Mahfouf, J.-F., and B. Jacquemin (1989), A study of rainfall interception using a land surface parameterization for mesoscale meteorological models, *J. Appl. Meteorol.*, 28, 1282–1302, doi:10.1175/1520-0450(1989)028<1282:ASORIU>2.0.CO;2.

Manzoni, S., and A. Porporato (2009), Soil carbon and nitrogen mineralization: Theory and models across scales, *Soil Biol. Biochem.*, 41, 1355–1379, doi:10.1016/j.soilbio.2009.02.031.

Marks, D., J. Kimball, D. Tingey, and T. Link (1998), The sensitivity of snowmelt processes to climate conditions and forest cover during rain-on-snow: A study of the 1996 Pacifc Northwest flood, *Hydrol. Processes*, 12, 1569–1587, doi:10.1002/(SICI)1099-1085(199808/09)12:10/11<1569::AID-HYP682>3.0.CO;2-L.

Marks, D., K. R. Cooley, D. C. Robertson, and A. Winstral (2000), Snow measurements and monitoring, Reynolds Creek Experimental Watershed, Idaho, USA, *Tech. Rep. 2000-5*, Northwest Watershed Res. Cent., Agric. Res. Serv., U.S. Dep. of Agric., Boise, Idaho.

Marks, D., K. R. Cooley, D. C. Robertson, and A. Winstral (2001), Long-term snow database, Reynolds Creek Experimental Watershed, Idaho, United States, *Water Resour. Res.*, 37(11), 2835–2838, doi:10.1029/2001WR000416.

Marks, D., A. Winstral, and M. Seyfried (2002), Simulation of terrain and forest shelter effects on patterns of snow deposition, snowmelt and runoff over a semi-arid mountain catchment, *Hydrol. Processes*, 16, 3605–3626, doi:10.1002/hyp.1237.

Martin, N., and S. M. Gorelick (2005), MOD_FreeSurf2D: A MATLAB surface fluid flow model for rivers and streams, *Comput. Geosci.*, 31, 929–946, doi:10.1016/j.cageo.2005.03.004.

Mascart, P., J. Noilhan, and H. Giordani (1995), A modified parameterization of flux-profile relationships in the surface layer using different roughness lengthvalues for heat and momentum, *Boundary Layer Meteorol.*, 72, 331–334, doi:10.1007/BF00708998.

Maxwell, R. M., and S. J. Kollet (2008), Quantifying the effects of three-dimensional subsurface heterogeneity on hortonian runoff processes using a coupled numerical, stochastic approach, *Adv. Water Resour.*, 31, 807–817, doi:10.1016/j.advwatres.2008.01.020.

Maxwell, R. M., and N. L. Miller (2005), Development of a coupled land surface and groundwater model, *J. Hydrometeorol.*, 6, 233–247, doi:10.1175/JHM422.1.

Maxwell, R. M., F. K. Chow, and S. J. Kollet (2007), The groundwater-land-surface-atmosphere connection: Soil moisture effects on the atmospheric boundary layer in fully-coupled simulations, *Adv. Water Resour.*, 30, 2447–2466, doi:10.1016/j.advwatres.2007.05.018.

McCree, K. J. (1970), An equation for the rate of respiration of white clover plants grown under controlled conditions, in *Proceedings of the Technical Meeting IBP, Trebon (CSK), 1969*, pp. 221–229, Pudoc, Wageningen, Netherlands.

Menduni, G., A. Pagani, M. C. Rulli, and R. Rosso (2002), A nonconventional watershed partitioning method for semi-distributed hydrological modelling: The package ALADHYN, *Hydrol. Processes*, 16, 277–291, doi:10.1002/hyp.340.

Millard, P., and G.-A. Grelet (2010), Nitrogen storage and remobilization by trees: Ecophysiological relevance in a changing world, *Tree Physiol.*, 30, 1083–1095, doi:10.1093/treephys/tpq042.

Mirus, B. B., B. A. Ebel, C. S. Heppner, and K. Loague (2011), Assessing the detail needed to capture rainfall-runoff dynamics with physics-based hydrologic response simulation, *Water Resour. Res.*, 47, W00H10, doi:10.1029/2010WR009906.

Mölders, N., H. Luijting, and K. Sassen (2008), Use of atmospheric radiation measurement program data from Barrow, Alaska, for evaluation and development of snow-albedo parameterizations, *Meteorol. Atmos. Phys.*, 99, 199–219, doi:10.1007/s00703-007-0271-6.

Molotch, N. P., P. D. Brooks, S. P. Burns, M. Litvak, R. K. Monson, J. R. McConnell, and K. Musselman (2009), Ecohydrological controls on snowmelt partitioning in mixed-conifer sub-alpine forests, *Ecohydrology*, 2, 129–142, doi:10.1002/eco.48.

Monin, A. S., and A. M. Obukhov (1954), Dimensionless characteristics of turbulence in the surface layer of the atmosphere [in Russian], *Trudy Geofiz. Inst. Akad. Nauk. SSSR*, 24, 163–187.

Montaldo, N., J. D. Albertson, and M. Mancini (2008), Vegetation dynamics and soil water balance in a water-limited Mediterranean ecosystem on Sardinia, Italy, *Hydrol. Earth Syst. Sci.*, 12, 1257–1271, doi:10.5194/hess-12-1257-2008.

Montgomery, D. R., and W. E. Dietrich (1988), Where do channels begin? *Nature*, 336, 232–234, doi:10.1038/336232a0.

Montgomery, D. R. and W. E. Dietrich (1989), Source areas, drainage density, and channel initiation, *Water Resour. Res.*, 25(8), 1907–1918, doi:10.1029/WR025i008p01907.

Mott, K. A. (1988), Do stomata respond to CO_2 concentrations other than intercellular? *Plant Physiol.*, 86, 200–203, doi:10.1104/pp.86.1.200.

Mualem, Y. and S. Assouline (1989), Modeling soil seal as a nonuniform layer, *Water Resour. Res.*, 25(10), 2101–2108, doi:10.1029/WR025i010p02101.

Mualem, Y., S. Assouline, and H. Rohdenburg (1990), Rainfall-induced soil seal. C. A dynamic model with kinetic energy instead of cumulative rainfall as independent variable, *Catena*, 17, 289–303, doi:10.1016/0341-8162(90)90022-6.

Nardi, F., S. Grimaldi, M. Santini, A. Petroselli, and L. Ubertini (2008), Hydrogeomorphic properties of simulated drainage patterns using digital elevation models: The flat area issue, *Hydrol. Sci. J.*, 53(6), 1176–1193, doi:10.1623/hysj.53.6.1176.

Noilhan, J., and J.-F. Mafhouf (1996), The ISBA land surface parameterisation scheme, *Global Planet. Change*, 13, 145–159, doi:10.1016/0921-8181(95)00043-7.

Nouvellon, Y., S. Rambal, D. L. Seen, M. S. Moran, J. P. Lhomme, A. Begue, A. G. Chehbouni, and Y. Kerr (2000), Modelling of daily fluxes of water and carbon from shortgrass steppes, *Agric. For. Meteorol.*, 100, 137–153, doi:10.1016/S0168-1923(99)00140-9.

O'Callaghan, J. F., and D. M. Mark (1984), The extraction of drainage networks from digital elevation data, *Comput. Vision Graphics Image Process.*, 28, 323–344, doi:10.1016/S0734-189X(84)80011-0.

Oleson, K. W., et al. (2004), Technical description of the community land model (CLM), *NCAR Tech. Note NCAR/TN-461+STR*, Natl. Cent. for Atmos. Res., Boulder, Colo.

Oleson, K. W., et al. (2008), Improvements to the Community Land Model and their impact on the hydrological cycle, *J. Geophys. Res.*, 113, G01021, doi:10.1029/2007JG000563.

Orlandini, S. (2002), On the spatial variation of resistance to flow in upland channel networks, *Water Resour. Res.*, 38(10), 1197., doi:10.1029/2001WR001187.

Orlandini, S. and G. Moretti (2009), Determination of surface flow paths from gridded elevation data, *Water Resour. Res.*, 45, W03417, doi:10.1029/2008WR007099.

Orlandini, S., G. Moretti, M. Franchini, B. Aldighieri, and B. Testa (2003), Path-based methods for the determination of nondispersive drainage directions in grid-based digital elevation models, *Water Resour. Res.*, 39(6), 1144, doi:10.1029/2002WR001639.

Orlandini, S., P. Tarolli, G. Moretti, and G. Dalla Fontana (2011), On the prediction of channel heads in a complex alpine terrain using gridded elevation data, *Water Resour. Res.*, 47, W02538, doi:10.1029/2010WR009648.

Panday, S., and P. S. Huyakorn (2004), A fully coupled physically-based spatially-distributed model for evaluating surface/subsurface flow, *Adv. Water Resour.*, 27, 361–382, doi:10.1016/j.advwatres.2004.02.016.

Paniconi, C. and E. F. Wood (1993), A detailed model for simulation of catchment scale subsurface hydrologic processes, *Water Resour. Res.*, 29(6), 1601–1620, doi:10.1029/92WR02333.

Pederson, C. A., and J.-G. Winther (2005), Intercomparison and validation of snow-albedo parameterization schemes in climate models, *Clim. Dyn.*, 25, 351–362, doi:10.1007/s00382-005-0037-0.

Pomeroy, J. W., N. Parviainen, N. Hedstrom, and D. M. Gray (1998), Coupled modeling of forest snow interception and sublimation, *Hydrol. Processes*, 12, 2317–2337, doi:10.1002/(SICI)1099-1085(199812)12:15<2317::AID-HYP799>3.0.CO;2-X.

Pomeroy, J. W., D. M. Gray, N. Hedstrom, and J. R. Janowicz (2002), Prediction of seasonal snow accumulation in cold climate forests, *Hydrol. Processes*, 16, 3543–3558, doi:10.1002/hyp.1228.

Porporato, A., F. Laio, L. Ridolfi, and I. Rodriguez-Iturbe (2001), Plants in water-controlled ecosystems: Active role in hydrologic processes and response to water stress III. Vegetation water stress, *Adv. Water Resour.*, 24, 725–744, doi:10.1016/S0309-1708(01)00006-9.

Porporato, A., P. D'Odorico, F. Laio, and I. Rodriguez-Iturbe (2003), Hydrologic controls on soil carbon and nitrogen cycles. I. Modeling scheme, *Adv. Water Resour.*, 26, 45–58, doi:10.1016/S0309-1708(02)00094-5.

Pregitzer, K. S. (2003), Woody plants, carbon allocation and fine roots, *New Phytol.*, 158(3), 421–424, doi:10.1046/j.1469-8137.2003.00766.x.

Qu, Y. and C. J. Duffy (2007), A semidiscrete finite volume formulation for multiprocess watershed simulation, *Water Resour. Res.*, 43, W08419, doi:10.1029/2006WR005752.

Quinn, P., K. Beven, P. Chevallier, and O. Planchon (1991), The prediction of hillslope flow paths for distributed hydrological modeling using digital terrain models, *Hydrol. Processes*, 5, 59–80, doi:10.1002/hyp.3360050106.

Quinn, P. F., K. J. Beven, and R. Lamb (1995), The ln(a/tanβ) index: How to calculate it and how to use in within the TOPMODEL framework, *Hydrol. Processes*, 9, 161–182.

Ramírez, J. A., and S. U. S. Senarath (2000), A statistical-dynamical parameterization of interception and land surface-atmosphere

interactions, *J. Clim.*, 13, 4050–4063, doi:10.1175/1520-0442(2000) 013<4050:ASDPOI>2.0.CO;2.

Reba, M. L., D. Marks, M. Seyfried, A. Winstral, M. Kumar, and G. Flerchinger (2011), A long-term data set for hydrologic modeling in a snow-dominated mountain catchment, *Water Resour. Res.*, 47, W07702, doi:10.1029/2010WR010030.

Reed, S., V. Koren, M. Smith, Z. Zhang, F. Moreda, D.-J. Seo, and DMIP Participants (2004), Overall distributed model intercomparison project results, *J. Hydrol.*, 298, 27–60, doi:10.1016/j.jhydrol. 2004.03.031.

Reich, P. B., M. B. Walters, and D. S. Ellsworth (1997), From tropics to tundra: Global convergence in plant functioning, *Proc. Natl. Acad. Sci. U. S. A.*, 94, 13,730–13,734.

Reich, P. B., M. B. Walters, D. S. Ellsworth, J. M. Vose, J. C. Volin, C. Gresham, and W. D. Bowman (1998), Relationships of leaf dark respiration to leaf nitrogen, specific leaf area and leaf life-span: A test across biomes and functional groups, *Oecologia*, 114, 471–482, doi:10.1007/s004420050471.

Reich, P. B., M. G. Tjoelker, J.-L. Machado, and J. Oleksyn (2006), Universal scaling of respiratory metabolism, size and nitrogen in plants, *Nature*, 339, 457–461, doi:10.1038/nature04282.

Rigon, R., G. Bertoldi, and T. M. Over (2006), GEOtop: A distributed hydrological model with coupled water and energy budgets, *J. Hydrometeorol.*, 7(3), 371–388, doi:10.1175/JHM497.1.

Rodriguez-Iturbe, I. (2000), Ecohydrology: A hydrologic perspective of climate-soil-vegetation dynamics, *Water Resour. Res.*, 36(1), 3–9, doi:10.1029/1999WR900210.

Rodriguez-Iturbe, I., and A. Porporato (2004), *Ecohydrology of Water-Controlled Ecosystems*, Cambridge Univ. Press, Cambridge, U. K.

Rodriguez-Iturbe, I., P. D'Odorico, A. Porporato, and L. Ridolfi (1999), On the spatial and temporal links between vegetation, climate, and soil moisture, *Water Resour. Res.*, 35(12), 3709–3722, doi:10.1029/1999WR900255.

Rodriguez-Iturbe, I., A. Porporato, F. Laio, and L. Ridolfi (2001), Plants in water-controlled ecosystems: Active role in hydrologic processes and response to water stress I. Scope and general outline, *Adv. Water Resour.*, 24, 695–705, doi:10.1016/S0309-1708(01)00004-5.

Ruimy, A., G. Dedieu, and B. Saugier (1996), TURC: A diagnostic model of continental gross primary productivity and net primary productivity, *Global Biogeochem. Cycles*, 10, 269–285, doi:10.1029/ 96GB00349.

Rulli, M. C. (2010), A physically based watershed partitioning method, *Adv. Water Resour.*, 33, 1206–1215, doi:10.1016/j.advwatres.2010. 06.011.

Rutter, A. J., K. A. Kershaw, P. C. Robins, and A. J. Morton (1971), A predictive model of rainfall interception in forests. 1. Derivation of the model from observation in a plantation of Corsican pine, *Agric. Meteorol.*, 9, 367–384, doi:10.1016/0002-1571(71)90034-3.

Rutter, A. J., A. J. Morton, and P. C. Robins (1975), A predictive model of rainfall interception in forests. 2. Generalization of model and comparison with observations in some coniferous and hardwood stands, *J. Appl. Ecol.*, 12(1), 367–380, doi:10.2307/2401739.

Ryan, M. G. (1991), Effects of climate change on plant respiration, *Ecol. Appl.*, 1(2), 157–167, doi:10.2307/1941808.

Sakaguchi, K., and X. Zeng (2009), Effects of soil wetness, plant litter, and under-canopy atmospheric stability on ground evaporation in the Community Land Model (CLM3.5), *J. Geophys. Res.*, 114, D01107, doi:10.1029/2008JD010834.

Sato, H., A. Itoh, and T. Kohyama (2007), SEIB-DGVM: A new Dynamic Global Vegetation Model using a spatially explicit individual-based approach, *Ecol. Modell.*, 200, 279–307, doi:10.1016/j. ecolmodel.2006.09.006.

Saxton, K. E., and W. J. Rawls (2006), Soil water characteristic estimates by texture and organic matter for hydrologic solutions, *Soil Sci. Soc. Am. J.*, 70, 1569–1578, doi:10.2136/sssaj2005.0117.

Schenk, H. J., and R. B. Jackson (2002), The global biogeography of roots, *Ecol. Monogr.*, 72(3), 311–328, doi:10.1890/0012-9615 (2002)072[0311:TGBOR]2.0.CO;2.

Schulze, E., F. M. Kelliher, C. Korner, J. Lloyd, and R. Leuning (1994), Relationships among maximum stomatal conductance, ecosystem surface conductance, carbon assimilation rate, and plant nitrogen nutrition: A global ecology scaling exercise, *Annu. Rev. Ecol. Syst.*, 25, 629–662, doi:10.1146/annurev.es.25.110194.00321.

Schwanghart, W., and N. J. Kuhn (2010), Topotoolbox: A set of Matlab functions for topographic analysis, *Environ. Modell. Software*, 25, 770–781, doi:10.1016/j.envsoft.2009.12.002.

Scott, R. L., W. J. Shuttleworth, T. O. Keefer, and A. W. Warrick (2000), Modeling multiyear observations of soil moisture recharge in the semiarid American Southwest, *Water Resour. Res.*, 36(8), 2233–2247, doi:10.1029/2000WR900116.

Sellers, P. J. (1985), Canopy reflectance, photosynthesis and transpiration, *Int. J. Remote Sens.*, 6, 1335–1372, doi:10.1080/0143116 8508948283.

Sellers, P. J., M. D. Heiser, and F. G. Hall (1992), Relations between surface conductance and spectral vegetation indices at intermediate (100m² to 15km²) length scales, *J. Geophys. Res.*, 97(D17), 19,033–19,059.

Sellers, P. J., D. A. Randall, G. J. Collatz, J. A. Berry, C. B. Field, D. A. Dazlich, C. Zhang, G. D. Collelo, and L. Bounoua (1996), A revised land surface parameterization (SiB2) for atmospheric GCMs. 1. Model formulation, *J. Clim.*, 9(4), 674–705.

Sellers, P. J., et al. (1997), Modeling the exchanges of energy, water and carbon between continents and the atmosphere, *Science*, 275, 502–509, doi:10.1126/science.275.5299.502.

Seyfried, M. S., M. D. Murdock, C. L. Hanson, G. N. Flerchinger, and S. Van Vactor (2001), Long-term soil water content database, Reynolds Creek Experimental Watershed, Idaho, United States, *Water Resour. Res.*, 37(11), 2847–2851, doi:10.1029/2001WR 000419.

Seyfried, M. S., L. E. Grant, D. Marks, A. Winstral, and J. McNamara (2009), Simulated soil water storage effects on streamflow generation in a mountainous snowmelt environment, Idaho, USA, *Hydrol. Processes*, 23, 858–873, doi:10.1002/hyp.7211.

Shuttleworth, W. J., and R. J. Gurney (1990), The theoretical relationship between foliage temperature and canopy resistance in sparse crops, *Q. J. R. Meteorol. Soc.*, 116, 497–519, doi:10.1002/ qj.49711649213.

Singh, V. P., and D. A. Woolhiser (2002), Mathematical modeling of watershed hydrology, *J. Hydrol. Eng.*, 7(4), 270–292, doi:10.1061/ (ASCE)1084-0699(2002)7:4(270).

Sitch, S., et al. (2003), Evaluation of ecosystem dynamics, plant geography and terrestrial carbon cycling in the LPJ dynamic global vegetation model, *Global Change Biol.*, 9, 161–185, doi:10.1046/j. 1365-2486.2003.00569.x.

Sivapalan, M., K. Beven, and E. F. Wood (1987), On hydrologic similarity: 2. A scaled model of storm runoff production, *Water Resour. Res.*, 23(12), 2266–2278, doi:10.1029/WR023i012p02266.

Skirvin, S., M. Kidwell, S. Biedenbender, J. P. Henley, D. King, C. H. Collins, S. Moran, and M. Weltz (2008), Vegetation data, Walnut Gulch Experimental Watershed, Arizona, United States, *Water Resour. Res.*, 44, W05S08, doi:10.1029/2006WR005724.

Slaughter, C. W., D. Marks, G. N. Flerchinger, S. S. Van Vactor, and M. Burgess (2001), Thirty-five years of research data collection at the Reynolds Creek Experimental Watershed, Idaho, United States, *Water Resour. Res.*, 37(11), 2819–2823, doi:10.1029/2001WR 000413.

Strack, J. E., G. E. Liston, and R. A. Pielke (2004), Modeling snow depth for improved simulation of snow-vegetation-atmosphere interactions, *J. Hydrometeorol.*, 5, 723–734, doi:10.1175/1525-7541(2004) 005<0723:MSDFIS>2.0.CO;2.

Strasser, U., M. Bernhardt, M. Weber, G. E. Liston, and W. Mauser (2008), Is snow sublimation important in the Alpine water balance? *Cryosphere*, 2, 53–66, doi:10.5194/tc-2-53-2008.

Tague, C. L. (2009), Assessing climate change impacts on alpine stream-flow and vegetation water use: Mining the linkages with subsurface hydrologic processes, *Hydrol. Processes*, 23, 1815–1819, doi:10.1002/hyp.7288.

Tague, C. L., and L. E. Band (2004), RHESSys: Regional Hydro-Ecologic Simulation System: An object-oriented approach to spatially distributed modeling of carbon, water, and nutrient cycling, *Earth Interact.*, 8(19), 1–42, doi:10.1175/1087-3562(2004)8<1: RRHSSO>2.0.CO;2.

Tarboton, D. G. (1997), A new method for the determination of flow directions and upslope areas in grid digital elevation models, *Water Resour. Res.*, 33(2), 309–319, doi:10.1029/96WR03137.

Tarboton, D. G., and C. H. Luce (1996), Utah Energy Balance snow accumulation and melt model (UEB): Computer model technical description and user's guide, technical report, Utah Water Res. Lab., Logan.

Tardieu, F., and W. J. Davies (1993), Integration of hydraulic and chemical signalling in the control of stomatal conductance and water status of droughted plants, *Plant Cell Environ.*, 16, 341–349, doi:10. 1111/j.1365-3040.1993.tb00880.x.

Thompson, S. E., C. J. Harman, A. G. Konings, M. Sivapalan, A. Neal, and P. A. Troch (2011a), Comparative hydrology across AmeriFlux sites: The variable roles of climate, vegetation, and groundwater, *Water Resour. Res.*, 47, W00J07, doi:10.1029/ 2010WR009797.

Thompson, S. E., C. J. Harman, P. A. Troch, P. D. Brooks, and M. Sivapalan (2011b), Spatial scale dependence of ecohydrologically mediated water balance partitioning: A synthesis framework for catchment ecohydrology, *Water Resour. Res.*, *47*, W00J03, doi:10.1029/2010WR009998.

Thornley, J. H. M. (1970), Respiration, growth and maintenance in plants, *Nature*, *227*, 304–305, doi:10.1038/227304b0.

Tromp-van Meerveld, I., and M. Weiler (2008), Hillslope dynamics modeled with increasing complexity, *J. Hydrol.*, *361*, 24–40, doi:10.1016/j.jhydrol.2008.07.019.

Tucker, G. E., S. T. Lancaster, N. M. Gasparini, R. L. Bras, and S. M. Rybarczyk (2001), An object-oriented framework for distributed hydrologic and geomorphologic modeling using triangulated irregular networks, *Comput. Geosci.*, *27*(8), 959–973, doi:10.1016/S0098-3004(00)00134-5.

Tuzet, A., A. Perrier, and R. Leuning (2003), A coupled model of stomatal conductance, photosynthesis and transpiration, *Plant Cell Environ.*, *26*, 1097–1116, doi:10.1046/j.1365-3040.2003.01035.x.

TVA (1972), Heat and mass transfer between a water surface and the atmosphere, *Tech. Rep. 14*, Tenn. Val. Auth. Water Resour. Res. Eng. Lab., Norris.

van den Hurk, B. J. J. M., and A. A. M. Holtslag (1997), On the bulk parameterization of surface fluxes for various conditions and parameter ranges, *Boundary Layer Meteorol.*, *82*, 119–134, doi:10.1023/A:1000245600901.

vanGenuchten, M. T. (1980), A closed-form equation for predicting the hydraulic conductivity of unsaturated soils, *Soil Sci. Soc. Am. J.*, *44*, 892–898, doi:10.2136/sssaj1980.03615995004400050002x.

Veatch, W., P. D. Brooks, J. R. Gustafson, and N. P. Molotch (2009), Quantifying the effects of forest canopy cover on net snow accumulation at a continental, mid-latitude site, *Ecohydrology*, *2*(2), 115–128, doi:10.1002/eco.45.

Vereecken, H., M. Weynants, M. Javaux, Y. Pachepsky, M. G. Schaap, and M. van Genuchten (2010), Using pedotransfer functions to estimate the van Genuchten-Mualem soil hydraulic properties: A review, *Vadose Zone J.*, *9*, 795–820, doi:10.2136/vzj2010.0045.

Verseghy, D. L. (1991), CLASS-A Canadian land surface scheme for GCMs. I. Soil model, *Int. J. Climatol.*, *11*, 111–133, doi:10.1002/joc.3370110202.

Vivoni, E. R., V. Y. Ivanov, R. L. Bras, and D. Entekhabi (2005), On the effects of triangulated terrain resolution on distributed hydrologic model response, *Hydrol. Processes*, *19*(11), 2101–2122, doi:10.1002/hyp.5671.

Wang, Y.-P., and R. Leuning (1998), A two-leaf model for canopy conductance, photosynthesis and portioning of available energy I: Model description and comparison with a multi-layered model, *Agric. For. Meteorol.*, *91*, 89–111, doi:10.1016/S0168-1923(98)00061-6.

Weiler, M., and J. J. McDonnell (2004), Virtual experiments: A new approach for improving process conceptualization in hillslope hydrology, *J. Hydrol.*, *285*, 3–18, doi:10.1016/S0022-1694(03)00271-3.

White, M. A., P. E. Thornton, S. W. Running, and R. R. Nemani (2000), Parameterization and sensitivity analysis of the BIOME-BGC terrestrial ecosystem model: Net primary production controls, *Earth Interact.*, *4*(3), 1–85, doi:10.1175/1087-3562(2000)004<0003:PASAOT>2.0.CO;2.

Wigmosta, M. S. and D. P. Lettenmaier (1999), A comparison of simplified methods for routing topographically driven subsurface flow, *Water Resour. Res.*, *35*(1), 255–264, doi:10.1029/1998WR900017.

Wigmosta, M. S., L. W. Vail, and D. P. Lettenmaier (1994), A distributed hydrology-vegetation model for complex terrain, *Water Resour. Res.*, *30*(6), 1665–1679, doi:10.1029/94WR00436.

Williams, K. S., and D. G. Tarboton (1999), The ABC's of snowmelt: A topographically factorized energy component snowmelt model, *Hydrol. Processes*, *13*, 1905–1920, doi:10.1002/(SICI)1099-1085(199909)13:12/13<1905::AID-HYP890>3.0.CO;2-#.

Winstral, A., and D. Marks (2002), Simulating wind fields and snow redistribution using terrain-based parameters to model snow accumulation and melt over a semi-arid mountain catchment, *Hydrol. Processes*, *16*, 3585–3603, doi:10.1002/hyp.1238.

Wood, E. F., et al. (2011), Hyperresolution global land surface modeling: Meeting a grand challenge for monitoring Earth's terrestrial water, *Water Resour. Res.*, *47*, W05301, doi:10.1029/2010WR010090.

Wramneby, A., B. Smith, S. Zaehle, and M. T. Sykes (2008), Parameter uncertainties in the modelling of vegetation dynamics-effects on tree community structure and ecosystem functioning in European forest biomes, *Ecol. Modell.*, *216*, 277–290, doi:10.1016/j.ecolmodel.2008.04.013.

Wright, I. J., et al. (2004), The worldwide leaf economics spectrum, *Nature*, *428*, 821–827, doi:10.1038/nature02403.

Zeng, X., R. Dickinson, M. Barlage, Y. Dai, G. Wang, and K. Oleson (2005), Treatment of undercanopy turbulence in land models, *J. Clim.*, *18*, 5086–5094, doi:10.1175/JCLI3595.1.

Corresponding author: S. Fatichi, Institute of Environmental Engineering, ETH Zürich, Wolfgang-Pauli-Str. 15, HIL D 23.2, CH-8093 Zürich, Switzerland. (simone.fatichi@ifu.baug.ethz.ch)